# A biomimetic fruit fly robot for studying the neuromechanics of legged locomotion

Bioinspiration & Biomimetics

PAPER

# A biomimetic fruit fly robot for studying the neuromechanics of legged locomotion

Clarus A Goldsmith[1,*], Moritz Haustein[2], Ansgar Büschges[2] and Nicholas S Szczecinski[1]

[1] Department of Mechanical, Materials and Aerospace Engineering, West Virginia University, Morgantown, WV, United States of America
[2] Institute of Zoology, University of Cologne, Köln, NRW, Germany
* Author to whom any correspondence should be addressed.

**E-mail:** cg00022@mix.wvu.edu

**Keywords:** Drosophila, walking, biomimetic, legged robot, neuromechanics

Supplementary material for this article is available online

OPEN ACCESS

RECEIVED
5 June 2024

REVISED
15 August 2024

ACCEPTED FOR PUBLICATION
27 September 2024

PUBLISHED
9 October 2024



## Abstract

For decades, the field of biologically inspired robotics has leveraged insights from animal locomotion to improve the walking ability of legged robots. Recently, 'biomimetic' robots have been developed to model how specific animals walk. By prioritizing biological accuracy to the target organism rather than the application of general principles from biology, these robots can be used to develop detailed biological hypotheses for animal experiments, ultimately improving our understanding of the biological control of legs while improving technical solutions. In this work, we report the development and validation of the robot Drosophibot II, a meso-scale robotic model of an adult fruit fly, *Drosophila melanogaster*. This robot is novel for its close attention to the kinematics and dynamics of *Drosophila*, an increasingly important model of legged locomotion. Each leg's proportions and degrees of freedom have been modeled after *Drosophila* 3D pose estimation data. We developed a program to automatically solve the inverse kinematics necessary for walking and solve the inverse dynamics necessary for mechatronic design. By applying this solver to a fly-scale body structure, we demonstrate that the robot's dynamics fit those modeled for the fly. We validate the robot's ability to walk forward and backward via open-loop straight line walking with biologically inspired foot trajectories. This robot will be used to test biologically inspired walking controllers informed by the morphology and dynamics of the insect nervous system, which will increase our understanding of how the nervous system controls legged locomotion.

## 1. Introduction

While scientists and engineers have increasingly realized the potential of robots to complete tasks in real-world environments, the design and control of legs has been a persistent topic of interest. Robots with legs can traverse natural and man-made terrains that are non-traversable with wheels or treads. However, their additional degrees of freedom (DoF) make them more mechanically complex and difficult to control. For the past several decades, the field of biologically-inspired robotics has used animal locomotion as a template [29, 40] to improve the capability of robots (for reviews, see [14, 45, 71, 103]). The structures of animal legs have evolved over hundreds of millions of years to traverse dynamic and uncertain terrains. Consequently, animal nervous systems are finely tuned to control these structures in a robust and adaptable manner. By applying principles from animal neuromechanics to robots, engineers are able to endow robots with similar capabilities and improve their locomotion. Such an approach has been successfully applied to many modes of locomotion including swimming [13, 46, 99], climbing [47, 76, 87], and flying [21, 54, 77] in addition to walking [26, 43, 65, 70].

More recently, a new, 'biology-first' approach to designing robots has developed to model how specific animals walk [9, 25, 32, 48, 73, 78, 96]. By closely modeling the neuromechanics of their target animal, these 'biomimetic' robots serve as both capable walking machines and testbeds for neuromechanical hypotheses. Scientists and engineers can then apply data collected from these robots to advance our incomplete understanding of the nervous system. For example, a biomimetic robot controlled by a walking controller created from biological data can be used to explore what is necessary and sufficient to control walking in the nervous system. In this way, developing biomimetic robots and using them for neuro-robotic investigations reciprocally benefits biology and robotics.

Insects have consistently been a target for bioinspired and biomimetic legged robotics due to their mechanical capability and amenability to neuromechanical study (reviews in [56, 72, 94, 104]). Despite the small size of their bodies and nervous systems, insects demonstrate a range of legged behaviors rivaling that of vertebrates. A variety of tools have been developed over the last 50+ years to investigate invertebrate nervous systems, providing a library of neurobiological insect data from which to develop robot controllers [10, 34, 61]. The hexapod structure of insects enables statically stable locomotion at all speeds without redundant legs, making them appealing models for robots [18, 92, 98]. Early insect-inspired robots near the end of the twentieth century leveraged these aspects of insects to produce robust walking through distributed controller architectures [12, 26, 90]. These early endeavors highlighted the benefits of a biologically-inspired approach in insect robots. As computational power advanced, similar insect robots began modeling the dynamics of neurons and synapses in their controllers to more closely model the neural control of walking [81, 89, 102].

As a result of the influx of biological data, a growing number of highly biomimetic insect robots have been developed with close consideration to both the nervous system and mechanics of their target animal. One example is the hexapod robot HECTOR, which was modeled after the stick insect, *Carausius morosus*. HECTOR's design uses the relative distances of the leg attachment points, the orientation of leg joint axes, and the division into three body segments to inform the mechatronic design [25, 82]. The robot has been used to explore several mechanical aspects of bioinspired locomotion such as compliant actuation and distributed proprioception, as well as serving as the testbed for the decentralized walking controller, Walknet [81]. Another example is ALPHA, a robot modeled after the African ball-rolling dung beetle *Scarabaeinae galenus*. ALPHA utilized Micro-CT scans of dead specimens to precisely proportion the legs and body [9]. Joint axes' positions and angles were also derived from these scans based on a series of cylinders and cones aligned with each joint's surface curvature. The researchers behind ALPHA demonstrated several mechanical benefits of the robot's biomimetic morphology compared to a traditional hexapod configuration, such as increasing possible step lengths and decreasing motor accelerations. These results provide motivation for copying the complexities of insect leg kinematics.

Although many insect species have been studied to unravel motor control of locomotion until today, the fruit fly, *Drosophila melanogaster*, has gained more and more popularity in the field of neurobiology over the last decades due to its tremendous potential to link behavior with the anatomy and physiology of the nervous system. There is accumulating knowledge about the anatomy of the brain and ventral nerve cord including several connectomes [66, 79, 80, 97]. The ever-growing genetic toolboxes available for *Drosophila* (for review: [15, 37, 53, 62, 101]) also enable recording neuronal activity in behaving animals [39] and to manipulate the activity of specific neurons in a straight-forward manner (e.g. [7, 8, 16, 27]). Further, several *Drosophila* studies have identified neurons similar to those found in other insects [2, 55], demonstrating the potential for data from other insects to be applied to *Drosophila*, and vice versa. All together these developments render *Drosophila* as a promising target organism for biomimetic insect robot construction.

Drosophibot [32], a meso-scale robot modeled after *Drosophila melanogaster*, was previously developed to further facilitate the testing of synthetic nervous system (SNS) controllers based on the insect nervous system [31, 64, 75, 96]. Drosophibot included several features to capture the animal's biomechanics such as biomimetic actuator control and sensing and parallel elastic joints. The robot was developed before 3D motion capture data for the fly was available, so leg proportions and joint axes were instead approximated from video footage and inspired by other insects such as *C. morosus*. Each leg was manufactured identically to simplify mechatronic design. As a result, several of the joint axes and leg attachment points were not accurate to the animal, so the robot struggled to execute fly-like walking.

Now that more neuromechanical data is available for *Drosophila* and recent advances in pose estimation algorithms allow the recording of 3D kinematic data at the leg joint level [35, 38, 57], we have designed a new robot that more closely resembles the insect to

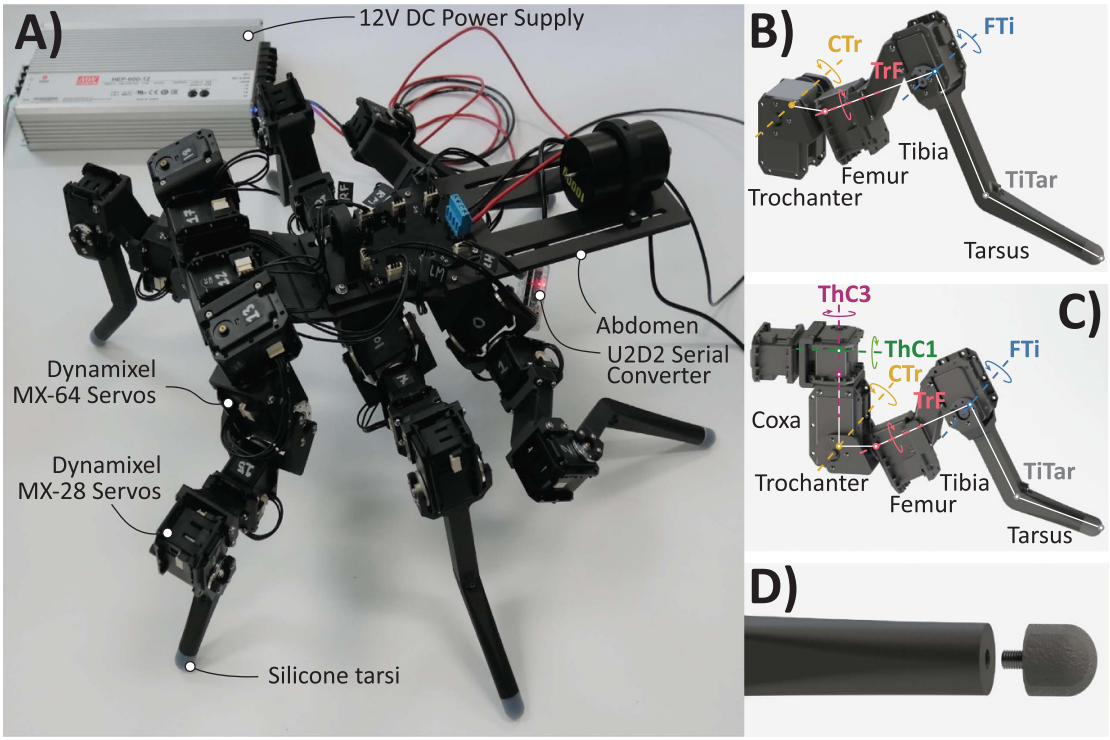


**Figure 1.** Drosophibot II, a biomimetic robot modeled after Drosophila melanogaster. (A) Photo of the robot with notable components annotated. (B) CAD rendering of a middle leg with the leg segments, joints, and axes of rotation labeled. The middle and hind legs have the same DoF and leg segments, though some segment lengths differ. (C) CAD rendering of a front leg with the leg segments, joints and axes of rotation labeled. (D) CAD rendering of the modular tarsus tip.

facilitate further investigations of the fly nervous system. In particular, we want the robot and the fly to be kinematically and dynamically similar. Kinematic similarity means that the robot's legs execute similar motions as the insect, which is crucial for investigating aspects of insect walking such as interleg coordination [19, 92, 105]. Dynamic similarity refers to similar force propogation as the fly in the robot's legs, as well as a similar combination of inertial, gravitational, elastic, and viscous forces acting within the legs. The interplay of these types of forces, which are tied to the animal's size and walking speed, has been found to significantly influence how the nervous system controls walking [1, 41, 91]. Ensuring the robot's kinematics and dynamics are similar to the animal prevents a brain-body mismatch while using SNS controllers for neuromechanical investigations. *Drosophila*'s nervous system has evolved over eons to control walking in a specific leg structure with sensory feedback tied to its dynamics. A SNS developed from *Drosophila* data will be naturally tuned to produce this type of control, so making the robot kinematically and dynamically similar despite its larger size prevents incongruities with the controller. Dynamic similarity will also enable us to investigate biomimetic sensory feedback during walking from sense organs such as the campaniform sensilla (CS), mechanoreceptors that encode exoskeleton strain [23, 59, 88].

### 1.1. Contributions

We present Drosophibot II, a biomimetic meso-scale robot modeled after the adult fruit fly, *Drosophila melanogaster*, to model and integrate the recent influx of *Drosophila* neuromechanical data (figure 1). Drosophibot II's leg proportions and DoF were closely modeled after 3D motion capture data from the insect performing straight line walking on a spherical treadmill. To our knowledge, it is the first biomimetic insect robot to utilize such data to inform its design. To design and validate the robot, we developed a program to generate biomimetic footpaths given key stepping parameters, solve the inverse kinematics necessary for walking, and calculate the inverse dynamics necessary to inform mechatronic design. We use this program to compare the joint angles and torques between the robot and a scale model of *Drosophila* and show that they are dynamically similar with and without parallel elastic components. We believe we are the first to apply such a rigorous consideration of dynamic similarity to the development of a biomimetic robot. The robot can successfully perform straight-line forward and

backward walking (Videos S1–2), as well as forward walking on an incline (Video S3). We also tested the robot at three different walking speeds to demonstrate that its walking is quasi-static, meaning that inertial forces do not impact its dynamics. This means that the weight of the actuators in the legs, which is not a biological mass distribution, does not meaningfully change the dynamics across walking speeds. In the future, this robot can be used to test walking controllers based on the neural control architecture of the insect nervous system, increasing our understanding of how the nervous system controls legs. Such knowledge can then be applied to further improve walking robots through the uncovering of locomotion principles.

## 2. Materials and methods

### 2.1. Fruit fly kinematics analysis

In order to closely characterize the kinematics of *Drosophila* on a robotic platform, we recorded tethered flies walking on a spherical treadmill (figure S1), then used DeepLabCut [57] to automatically annotate the recordings and for each trial. Appendix I in the Supplemental Materials describes this experimental setup and data collection in detail.

The pose estimation data tracks the spatial location of each joint in the legs (i.e. 'joint-points'), as well as additional body parts required to transform the positional data into a body-centered coordinate system. We then used this data to analyze the kinematics of the different leg pairs. In particular, we were interested in identifying the minimum number of DoF that best approximates the movement in each of the fly's leg pairs, as well as finding the average proportions between the different leg segments and leg attachment point distances on the body (e.g. the lateral distance between each pair of thorax-coxa (ThC) joints). By minimizing the number of actuated joints on the robot, we are able to minimize its overall actuator weight and increase its strength-to-weight ratio while enabling it to produce motions similar to those of the animal (e.g. walking in a line). Obtaining average leg and body ratios enabled us to construct the robot with 'typical' fly proportions (i.e. kinematic similarity).

Our method for the analysis of leg DoF is presented in detail in [30] where it was applied to the middle and hind leg pairs. To briefly summarize the process, we begin by constructing a mathematical kinematic leg chain for every frame of motion capture data, normalized such that the ThC is the origin of the leg's spatial frame. The leg chain contains seven total DoF that have been directly recorded orhypothesized to exist in the fly or other insects: ThC protraction/retraction (ThC1), levation/depression (ThC2), and rotation (ThC3); coxa-trochanter (CTr) flexion/extension; trochanter-femur (TrF) rotation (TrF1) and flexion/extension (TrF2); and femur-tibia (FTi) flexion/extension [52, 85, 86]. We use product of exponentials [60] to generate the leg chain with segment lengths calculated anew for each frame. We then find the 'best fit' configuration of the model by solving for the joint angles that minimize the sum of Euclidean distances between each joint-point in the model and on the animal. After completing this process for the 'complete' leg chain, various combinations of DoF were fixed at their average angle across an experimental trial to observe the effects these DoF have on the fit to the animal data. In that regard, we analyzed the average error in Euclidean distance of each joint-point as well as the average orientation and overall range of motion (RoM) of the 'leg plane' (i.e. the plane containing the femur and tibia major axes, figure S2). Orientation of the leg plane dictates the degree that moments from the ground reaction forces (GRF) are counteracted by the actuator versus passively resisted by reaction forces in the joint. Thus, considering the leg plane angle allowed us to consider biological force distributions.

Based on this method of analysis, we selected the CTr, TrF1, and FTi DoF as the mobile joints in our robot's middle and hind leg pairs (figure 1(B)) [30]. We then conducted analysis of the front limbs, as presented in figure S2. In addition to minimizing the number of actuators, for the front limbs we were interested in DoF combinations that would: (1) minimize the DoF in the ThC and (2) include the TrF1. The former criterion would help minimize the mechatronic complexity of the ThC on the robot, as fewer actuators would need to fit into the limited space. The latter criterion allows us to investigate the role of the TrF1 DoF in leg pronation/supination, as we have in the middle and hind limbs. In regards to the mean error of each joint-point (figure S2(A)), fixing only the ThC2 produced the least error across all joints. The mean error of the leg plane angle to the vertical (figure S2(B)) for this combination of fixed DoF was on average 8 degrees higher than in the animal. However, a similar level of error occurred in every DoF combination tested. The RoM of the leg plane was higher than that in the animal (figure S2(C)), but was considered inconsequential. Based on this analysis, we included the ThC1, ThC3, CTr, TrF, and FTi DoF in Drosophibot II's front legs (figure 1(C)), for five total DoF.

In addition to the DoF kinematic analysis, we determined the average proportions of the leg segments and body dimensions from our recorded flies ($N = 4/3$ females/males). We first calculated the distances between the joint-points for each frame of video capture to estimate leg segment lengths. These values were averaged over a trial to determine approximate lengths in each fly, then averaged again to calculate the segment lengths of a 'prototypical' fly. We scaled our robot such that the length of a middle leg

femur was 10 cm. As such, we used our 'prototypical' femur length in the fly data to determine length ratios between the femur and the other segments. Using these ratios, we calculated the leg segment lengths necessary for the robot to be proportional to the fruit fly. With a 10 cm femur length, Drosophibot II is approximately 140:1 scale to the insect.

### 2.2. Inverse kinematic and dynamic solver

Using the leg and body proportions and the selected DoF from the kinematic analysis, we then created an inverse kinematic and dynamic solver in MATLAB (MathWorks, Natick, MA). Figure 2 presents a visualization of the general workflow of this solver. The primary purposes of the solver were to generate robot limb trajectories given the body's motion through space [93] and calculate the joint torques, internal forces, and GRF in the robot during walking. Limb trajectories (e.g. joint angles necessary to move the foot in a particular way) can be used to control the robot, while aspects of the dynamics would inform actuator selection, power supply selection, and component design. The solver is capable of calculating these values for two different terrain shapes: a flat plane and ball. These terrains correspond to our desired use-case for the robot, and the biological data collection setup, respectively.

The solver begins by extracting position, dimension, and mass data (i.e. joint locations, axes, and limits; segment lengths, center of mass (CoM) locations, and masses) for each component of an organism's structure from a user provided Animatlab [17] file (figure 2(A)). We use 'organism' as a more general term to describe a given structure, as the solver may also be used to model animals. Using this provided structure, the solver generates a resting posture for the organism (figure 2(B)). Specifically, for a flat plane terrain it attempts to set each joint's angle close to the middle of its limits such that the foot's vertical ($y$) component is at a user defined ground level and that the lateral ($z$) and sagittal ($x$) components satisfy positional constraints in relation to the leg's ThC location adapted from the *Drosophila* stepping data [92]. For a ball terrain, the solver uses the same $x$ and $z$ coordinates as in the flat-plane posture, then projects these coordinates onto a sphere of a user-defined radius and vertical distance below the organism's CoM to calculate the $y$ coordinates.

Once a resting posture is found, the solver utilizes user-defined stepping parameters of walking speed, body translation and rotation per step, swing duration, and duty cycle to design stance-phase footpaths in each leg (figure 2(C)). The resting posture is used as the mid-point of these footpaths. A full list of the required parameters, as well as the values used to generate the data in this manuscript, can be found in table 1. Several of these parameters have previously been shown to be sufficient to predict biomimetic footpaths based on the desired movement of the body [93]. Using these footpaths, swing phase foot trajectories are calculated for the $x$, $y$, and $z$ components separately as 5th order polynomials. Figure S3 shows a representative footpath resulting from this interpolation, as well as the stance phase trajectories for all six legs of the robot. For the $x$ and $z$ components, one 5th order polynomial is generated between the start and end of stance (points 1 and 3 in figure S3(A)). For the $y$ component, two polynomials are used; one interpolated between the start of stance and a user specified peak swing height (points 1 and 2 in figure S3(A)), and the other between the swing peak and the end of stance (points 2 and 3 in figure S3(A)). Currently, the horizontal location of the peak swing height is set to the middle of the stance footpath.

#### 2.2.1. Inverse kinematics

Once a full foot trajectory has been generated, the solver performs inverse kinematics to find the joint angles necessary to complete the desired motions across the step (figure 2(D)). We chose to express the motion of the foot as a series of velocities in the body's frame of reference, used each leg's manipulator Jacobian to calculate the resulting joint angular velocities, then integrated these velocities to generate a trajectory of planned joint angle commands for the servomotors. This process was previously described in [93]. Because the change in configuration in this method is a linear approximation, error accumulates along the trajectory and the end will not exactly match the beginning. To join these ends without discontinuous motions (which produce large impulse forces in the inverse dynamics calculations), the first and final 30 points are replaced by a cubic interpolation between the 16th and $n$-15th points, where n is the total number of points. This process is repeated for each leg in the organism.

If the organism is configured to include parallel elastic elements, the solver additionally calculates equilibrium angles for each joint using the full RoM over the step. These values are tuned to produce leg positions resembling those of a newly dead fly, as such positions are the result of purely passive joint forces.

Once the joint angles, joint spatial positions, and leg segment CoM positions are calculated for each leg and for each timestep using the above method, the magnitudes of the angular velocity, $\dot{\theta}_{L,j,t}$ (where $L$ is the leg number, $j$ is the joint number, and $t$ is the slice number out of $n$ of the stepping cycle with duration $\Delta t = T_{sw}/n$) and angular acceleration, $\ddot{\theta}_{L,j,t}$ for each joint were calculated for each timestep as:

$$\dot{\theta}_{L,j,t} = \frac{\theta_{L,j,t+1} - \theta_{L,j,t-1}}{2\mathrm{d}t} \quad (1)$$

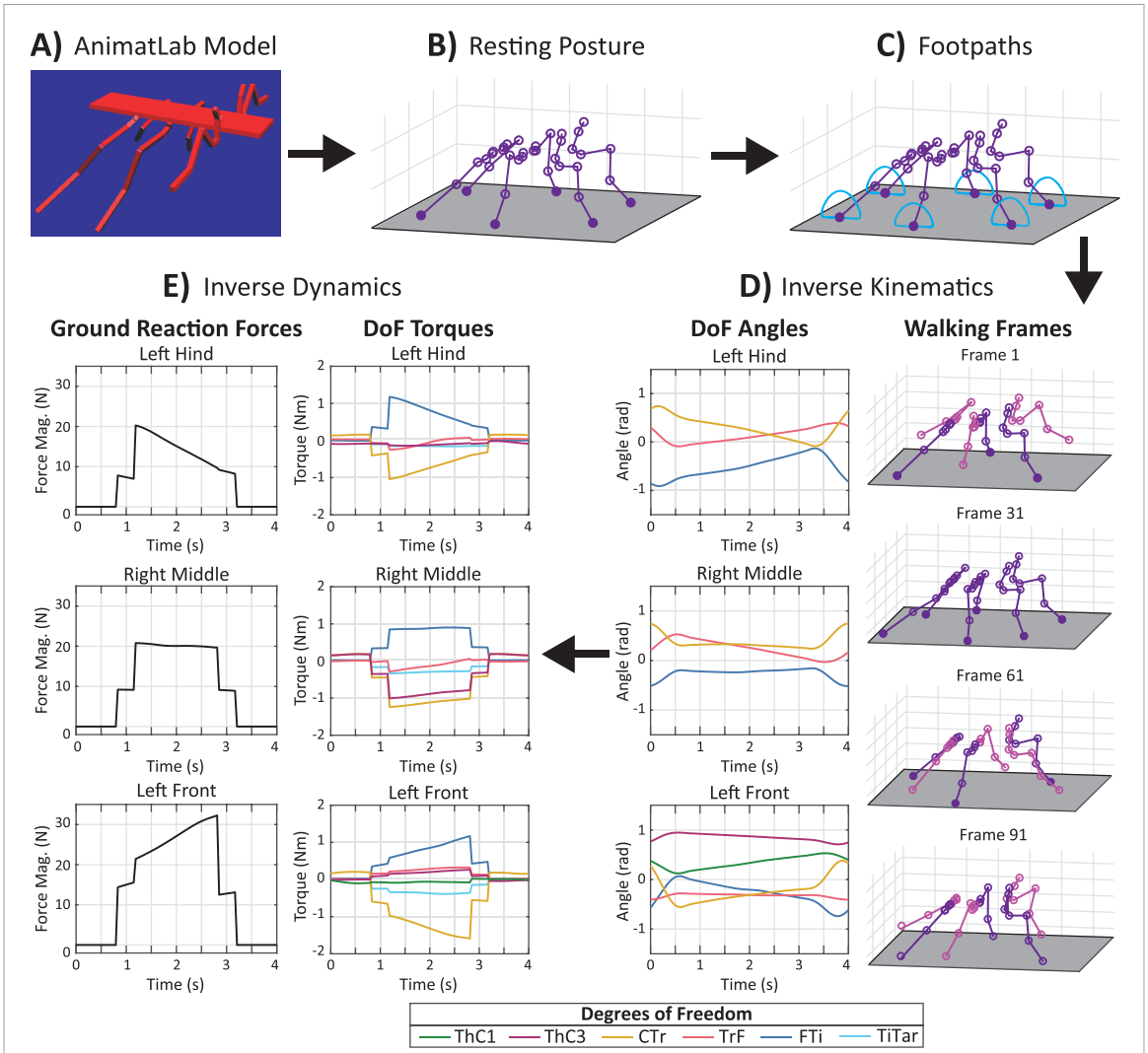


**Figure 2.** A representation of the workflow of our solver. (A) The user first provides an AnimatLab [17] file containing the organism structure. (B) The solver generates a resting posture using user provided body height and AnimatLab joint limits. (C) Using the rest posture as the midpoint, footpaths are generated using polynomial interpolation. (D) Inverse kinematics are calculated for each point in the footpath. (E) Inverse dynamics are calculated for each body in the organism for each timestep using the Newton–Euler equations of motion.

**Table 1.** Walking parameters of Drosophibot II and Scale-*Drosophila*. These values result in total step period of between 1 s–4 s for Drosophibot II, and 0.275 s for Scale-*Drosophila*. Body height is varied between leg pairs while physically running the robot to counteract servo backlash and component deformation.

| | | Value | | | |
|---|---|---|---|---|---|
| | | Drosophibot II | | | |
| Param. | Description | Hind | Middle | Front | Scale-*Drosophila* |
| $T_{sw}$ | Swing duration | | 0.4 s–1.6 s | | 0.1 s |
| $DS_{st}$ | Stance duty cycle | | 0.6 | | 0.6 |
| $h_{st}$ | Stance height | 0.07 m | 0.05 m | 0.09 m | 0.5 mm |
| $Tr_{body}$ | Body translation per step | | 0.085 m | | 0.6 mm |
| $h_{body}$ | Body height | 0.175 m | *Model*: 0.175 m *Robot*: 0.19 m | 0.175 m | 1.3 mm |

$$\ddot{\theta}_{L,j,t} = \frac{\dot{\theta}_{L,j,t+1} - \dot{\theta}_{L,j,t-1}}{2\mathrm{d}t} \tag{2}$$

where d$t$ is the amount of time in seconds each slice takes. If $t = 1$, the values for $t = n$ are used in place of those for $t - 1$. Similarly, if $t = n$ the values for $t = 1$ are used in place of those for $t + 1$.

Using these scalar values, the angular velocity vector for the CoM of each leg segment $s$, $\vec{\omega}_{L,s,t}$ is calculated as:

$$\vec{\omega}_{L,s,t} = \sum_{k=1}^{s} \dot{\theta}_{L,k,t}\vec{u}_{L,k,t} \tag{3}$$

where $\vec{u}_{L,k,t}$ is the joint axis of joint $j$ in leg $L$ at slice $t$, as measured in the global frame of reference. For each leg segment, the corresponding $j$ value is for the segment's proximal joint. For example, $s = 3$ corresponds to the femur, while $j = 3$ corresponds to the TrF. This angular velocity value is then used to calculate the angular acceleration vector for each segment, $\vec{\alpha}_{L,s,t}$:

$$\vec{\alpha}_{L,s,t} = \ddot{\theta}_{L,s,t}\vec{u}_{L,j,t} + \sum_{k=1}^{s-1}\left(\dot{\theta}_{L,k,t}\vec{u}_{L,k,t}\right) \times \vec{u}_{L,j,t}. \tag{4}$$

For the translational kinematics, the linear velocity of each segment's CoM, $\vec{v}_{L,s,t}$, is calculated as:

$$\vec{v}_{L,s,t} = \frac{\vec{r}_{L,s,t+1} - \vec{r}_{L,s,t-1}}{2\mathrm{d}t} \tag{5}$$

where $\vec{r}_{L,s,t}$ is the position of the segment's CoM with respect to the origin of the spatial frame. The translational acceleration is similarly calculated as:

$$\vec{a}_{L,s,t} = \frac{\vec{v}_{L,s,t+1} - \vec{v}_{L,s,t-1}}{2\mathrm{d}t}. \tag{6}$$

*2.2.2. Inverse dynamics*

Finally, the solver performs inverse dynamic calculations to determine the forces $\vec{F}$ and torques $\vec{T}$ acting on each leg segment and the thorax for each timestep (figure 2(E)). The solver shifts the phase of several of the joint angle arrays to produce the desired gait (e.g. for a tripod, 180 deg shift in one front leg, the contralateral middle leg, and the ipsilateral hind leg). If the organism includes parallel elastic components, the restoring torque for each timestep is calculated using the equilibrium positions defined during the inverse kinematic calculations.

The 3D translational and angular Newtonian equations of motion (EoM) are then constructed for each segment of each leg, as well as the thorax. A Newtonian formulation was used in lieu of Lagrangian to facilitate the calculation of internal reactions for each time step in addition to external forces. The equations are separated into $x$, $y$, and $z$ components and assembled into a series of matrices in the form $Ax = b$ for solving:

$$A\begin{bmatrix}\vec{F}\\ \vec{T}\end{bmatrix} = \begin{bmatrix}m\vec{a}\\ \frac{\mathrm{d}}{\mathrm{d}t}\vec{H}\end{bmatrix} \tag{7}$$

where $m$ is the mass of each segment, $\vec{a}$ is the linear acceleration, $\vec{H}$ is the angular momentum, and A is a matrix containing all of the coefficients of the force and torque variables in the left-hand sides of the EoM. Each segment's portion of A, which we refer to as 'building-blocks,' takes the form:

$$A_{L,s} = \begin{bmatrix} -I & I & 0 & 0\\ -\hat{r}_{L,s,j+1,t} & \hat{r}_{L,s,j,t} & -I & I\end{bmatrix} \tag{8}$$

where $I$ is the $3 \times 3$ identity matrix and $\hat{r}_{L,s,j,t}$ is the $3 \times 3$ skew matrix of the distance vector $\vec{r}_{L,s,j,t}$ between the CoM of the segment and the segment's proximal joint [60]. Similarly, $\hat{r}_{L,s,j+1,t}$ is the $3 \times 3$ skew matrix of the distance vector between the CoM of the segment and the segment's distal joint. The robot has 33 rigid bodies and 22 hinge joints, so assembling these building-blocks together results in 192 EoM and 210 unknown forces and torques (i.e. a $192 \times 210$ matrix). To ensure appropriate GRFs during swing, we additionally add $3L_{\mathrm{st}}$ equations to A, where $L_{\mathrm{st}}$ is the number of feet in swing, with the GRF of legs in swing explicitly set to zero. The thorax was assumed to only be moving at constant forward velocity to simplify calculations. With this number of equations and unknowns, the problem is underdetermined, and the forces and moments must be calculated by minimizing some objective function subject to the constraint that the EoM are satisfied. Our objective function represents the complementary potential energy $V^*$ of the system [100]:

$$V^* = \frac{1}{2}\sum_{i=0}^{J}\frac{T_{\mathrm{act},i}^2}{k_{\mathrm{joint},i}} = \frac{1}{2}\sum_{i=0}^{J}\frac{\left(\vec{u}_{\mathrm{joint},i}\cdot\vec{T}_{\mathrm{joint},i}\right)^2}{k_{\mathrm{joint},i}}. \tag{9}$$

In this equation, $T_{\mathrm{act}}$ is the torque output for each actuated joint, $k_{\mathrm{joint}}$ is the stiffness in the joint from the actuator's proportional feedback controller and any optional parallel elastic components, $\vec{u}_{\mathrm{joint}}$ is the joint axis for the selected joint, and $\vec{T}_{\mathrm{joint}}$ is the moment at the joint in the spatial frame. The stiffness in our chosen family of actuators, the Dynamixel MX series servos, was characterized for these calculations based on the process presented in [3]. By summing these values for the total number of actuated joints, $J$, created an equation that reflects both the actuator torques and the inherent elasticity in the system. Minimizing this value then minimizes the actuator torque while considering these other values. The program then minimizes equation (9) using the MATLAB function fmincon(), using $\vec{x}_0 = \vec{0}$ as the start point and the EoM as linear constraints. Once values are found, $T_{\mathrm{act}}$ is calculated by taking the dot

product of each joint's torque, $\vec{T}_{L,j}$, and $\vec{u}_{L,j}$. This process is repeated for every time slice.

The final output of our solver is joint angles, velocities, and accelerations, leg segment and thorax internal forces, joint torques, and GRF for each timestep throughout a single step cycle. The only required inputs to the system are those summarized in table 1. These data can then be concatenated to produce data for multiple steps. The joint angle data can be sent to the robot as commands for the servomotors. The dynamics data enabled us to carefully design the physical robot's mechanical strength, i.e. the torque each actuator must deliver during walking.

### 2.3. Comparison model generation

In order to validate the biomimicry of Drosophibot II, we created an additional *Drosophila*-like model to run through our solver framework. This model, called, 'Scale-*Drosophila*,' is a to-scale model of the fly based on the leg and thorax dimensions calculated as part of the kinematic analysis in section 2.1 and presented in table 2. In the robot, some dimensions were altered from the animal kinematics for mechatronic feasibility (see section 2.4 for more details); these dimensions were retained at their measured values for Scale-*Drosophila*. Additionally, each ThC joint was given the mobility observed in the animal, resulting in six total DoF per leg. The mass of this model was also distributed in a more animal-like way: In *Drosophila*, the abdomen, head, and thorax make up the bulk of the insect's mass, with the legs only comprising around 11% of the total [92]. By contrast, the weight of Drosophibot II's actuators results in 27% of the total weight distributed throughout the legs. To match the insect distribution in Scale-*Drosophila*, we distributed the mass of a female fly (as reported in [105]) using the percentages in [92]. The CoM of the thorax, head, and abdomen were set at the same location as found in [92]. The 11% of mass allocated to the legs was distributed throughout the leg segments proportional to each segment's length. These considerations result in Scale-*Drosophila* being a fully proportional fly analog. As GRF data from the animal is not presently available, this model allowed us to approximate force data and directly compare the dynamics of the animal and robot.

### 2.4. Robot construction

Drosophibot II is a hexapod robot with 22 actuated DoF developed using our inverse kinematic and dynamic solver (figure 1(A)). Each leg is segmented similarly to the leg segments of *Drosophila*, with a varying number of joints actuated within each leg pair. The middle and hind pairs of legs have three DoF, corresponding to the CTr, TrF, and FTi joints (figure 1(B)). The front legs have an additional two DoF for the ThC1 and ThC3 to enable the more complex motions *Drosophila*'s front limbs undergo during walking (figure 1(C)). DoF that were omitted from the robot's legs were fixed at their average position during the kinematic analysis (see previous sections and [30]). Each joint is actuated by a Dynamixel MX-series smart servo (Robotis, Seoul, South Korea); MX-28s are used for most joints, while MX-64s are used for the CTr due to the increased torque requirement at this joint. Using a single rotary actuator centered on the DoF axis differs from biological systems, which use antagonistic muscle pairs anchored on more proximal segments via tendons and ligaments to actuate leg DoF. However, we have shown in a previous study that the servomotors' internal controller can be tuned to behave dynamically similarly to an insect leg joint [95]. As such, this actuation scheme can be used without detracting from the biomimicry of the robot.

The majority of Drosphibot II's components are 3D printed out of Onyx composite nylon (Markforged, Waltham, MA). The distal end of each tarsal segment includes a threaded insert that allows for the tarsal tips to be unthreaded from the tarsus and swapped for other designs to best suit the robot's present terrain (figure 1(D)). For the data collection in this work, two different tarsal tips were used: a 3D printed Onyx core coated with a layer of Dragon Skin 10 silicone rubber (Smooth-On Inc. Macungie, PA), and a Flexible 80A Resin (Formlabs, Somerville, MA) tip with an Onyx 'cap.' The silicone and resin printed plastic both increase the robot's traction on our chosen substrates.

The robot's leg segments were designed such that their relative proportions were similar to those of *Drosophila* with the length of the femur set to 10 cm. This constraint results in the robot being approximately 140:1 scale to the insect. Table 2 compares leg segment lengths of Drosophibot II with the scaled-up average dimensions of the *Drosophila* specimens recorded as part of our kinematic analysis. Table S1 compares the dimensions between ThC joints (or where the ThC would be) on the thorax. In general, Drosophibot II's leg segment lengths are within 16% of a 140:1 Scale-*Drosophila*. The lengths that are not within these margins had to be modified due to mechanical constraints. For example, the trochanter was lengthened to the minimum distance necessary for the bracket to rotate around the body of the servo. The lengths that were modified are indicated by asterisks (*) in table 2. In the case of the thorax, when one dimension was modified, all other dimensions were similarly scaled such that the overall thorax proportions were consistent. For example, the lateral distance between the middle leg pair ThC joints was lengthened from 10.00 mm to 102.10 mm because this was the minimum distance possible without the servos for the middle limb CTr joints colliding. The

**Table 2.** Leg segment lengths of Drosophibot II and a 140:1 scaled *Drosophila*. *Drosophila* segment lengths were averaged from fly 3D motion capture data then scaled such that the middle leg femur was 100 mm. Dimensions from Drosophibot II marked with * were lengthened due to mechatronic constraints.

| | Drosopibot II value (mm) | | | Scaled *Drosophila* value (mm) | | | Percent error | | |
|---|---|---|---|---|---|---|---|---|---|
| Segment | Hind | Middle | Front | Hind | Middle | Front | Hind | Middle | Front |
| Coxa | — | — | 54.50 | 19.96 | 12.77 | 49.34 | — | — | 10.46 |
| Trochanter | 27.97* | 27.97* | 27.97* | 9.684 | 9.851 | 6.372 | 188.8 | 183.9 | 339.0 |
| Femur | 100.4 | 100.4 | 80.00 | 95.83 | 100.0 | 78.43 | 4.769 | .4000 | 2.041 |
| Tibia | 97.85 | 97.85 | 77.84 | 94.43 | 90.48 | 67.45 | 3.622 | 8.145 | 15.40 |
| Tarsus | 120.0 | 100.0 | 69.60 | 119.0 | 99.96 | 79.33 | .8403 | .0400 | 12.27 |

lateral distances between the front and hind limbs were then also extended by approx. 92 mm to keep the lateral distances between the ThC pairs scaled similarly to the animal. Each leg was affixed to the thorax such that the CTr joints were approximately within the same horizontal plane.

Because 45% of *Drosophila*'s mass is in its abdomen, the CoM of Drosophibot II's thorax and legs is much farther forward than in the insect. Previous investigations have calculated the anterior-posterior location of the insect's CoM as between the middle and hind legs [92], while Drosophibot II's CoM naturally falls between the middle and front legs. To shift the CoM to a more biological location, we have included an abdominal segment on Drosophibot II with slots for additional weight. We have found that including 1 kg of mass approximately 125 mm from the end of the thorax is enough to shift the CoM to an animal-like position. While adding mass does increase the load on the actuators, particularly in the hind legs, the robot's strength-to-weight ratio is such that the required joint torques are still well within the operating limit of the servos. This weight is presently provided by a 1 kg lab weight, but could be replaced by more functional ballast (e.g. batteries, sensors, control boards) in the future.

The robot is powered by an external Mean Well HEP-600-12 power supply (Mean Well Enterprises Co., Ltd New Taipei City, Taiwan) able to supply up to 40 A at 12 V. Power is routed from the supply to each servo by a custom circuit board. This board also includes communication traces to the servos. Presently, control signals are provided by an external laptop through a U2D2 serial converter (Robotis, Seoul, South Korea) connected to the power board. The laptop runs a MATLAB script that writes servo angle commands formulated by the kinematic solver to each servo. The script then reads the present servo angles, as well as the current draw of each servo. This current draw is converted into torque based on ratios presented in the Dynamixel E-Manuals. The read-write loop runs at 35 Hz.

### 2.5. Walking experiments

To validate the performance of Drosophibot II after manufacture and assembly, we conducted experiments in which the robot walked forward and backward in a straight-line on a flat plane, as well as walking forward up a 15° incline. These experiments were designed to test locomotion regimes of interest in *Drosophila* and other insects [8, 20, 108]. Experiments were conducted on a sand-paper substrate in the Neuromechanical Intelligence Lab at West Virginia University in Morgantown, WV. The robot was sent joint angle commands from our inverse kinematic solver and returned each servo's actual joint angle and measured current (as an approximation of joint torque) back to the control computer. It is presently unclear how accurate these current measurements are for the ground-truth, instant-to-instant joint torque. However, they are sufficient to provide general comparisons between different stepping scenarios of the physical robot. While our solver does output GRFs as part of the inverse dynamic calculations, GRFs are presently not collected from the physical robot.

To account for differences in component rigidity between the solver and the physical platform (e.g. gear backlash, 3D printed material elasticity, foot slippage) causing unwanted deflections and sagging, two solutions were implemented. First, parameters such as floor level were changed from those used for the robot in the idealized solver environment (table 1). Second, a bias term was added to the solved joint angles before being sent to the robot equal to the solved expected torque divided by the stiffness coefficient of the actuator (i.e. the proportional feedback gain, scaled to Nm rad$^{-1}$). These changes brought the posture of the robot closer to the planned posture.

During these walking experiments, the robot was commanded to step at periods between 1 s–4 s. This range of walking speed was selected to dynamically scale the motions of the robot to those of the insect. Due to the robot's much larger size, the robot will naturally have a different balance of viscous, elastic, and inertial forces present during stance and swing than *Drosophila*. Changing the walking speed can shift these values into a regime more similar to the

animal [91]. Detailed dynamic scaling calculations are presented in appendix II. The robot walked for 10 steps for the flat plane tests, and 5 steps for the incline tests.

## 3. Results

### 3.1. Simulation experiments

In order to evaluate the biomimicry of our robot, we kinematically and dynamically compared Drosophibot II to our Scale-*Drosophila* model in our solver. For these calculations, the modeled robot walked with a period of 4 s and the animal model walked with a period of 0.1 s (full stepping parameters can be found in table 1). The chosen parameters produce interleg coordination used by flies at intermediate walking speeds, which is neither a pure tripod nor tetrapod [92, 105]. A representative footfall pattern for all six legs in this coordination pattern is presented in figure S5.

#### *3.1.1. Robot and fly kinematic comparison*

Figure 3 qualitatively compares the kinematics of each mobile DoF in one tripod of a hind, middle, and front leg of Drosophibot II (solid lines) and Scale-*Drosophila* (dashed lines) during a single step on a flat plane using the same footpaths scaled to each organism's size. To aid in comparison, DoF that perform similar motions in the leg (e.g. both the ThC2 and CTr levate/depress the leg) are grouped on the same plot for both figures. Figure S6 presents similar kinematic analysis on a ball. Tables S2 and S3 present the coefficient of determination (R-squared) values for the linear regression of the modeled kinematics for each common DoF between the two organisms.

For Scale-*Drosophila*, the ball radius and position closely correspond to those from the biological data collection setup ($r = 3$ mm, $\Delta$y from CoM $= -3.7$ mm) [6]. For Drosophibot II, the ball parameters were normalized by the average of the body length and tibia length and scaled to produce a radius of 0.637 m and a vertical distance of $-0.76$ m from the CoM.

Differences in kinematics across both substrates can be explained by differing numbers of DoF and the curvature of the substrate. For the flat plane case, the change in angles in some DoF present across both organisms is negligibly small. The FTi angles in the hind and middle legs for both terrains are within 0.2 rad of each other throughout the step (figures 3(Aiii) and (Biii)). The ThC1 angle in the front legs (figure 3(Ci)) shows similarly small variation. In shared DoF with larger discrepancies, the majority exhibit similar trajectories and RoM over the step; the mid-point of that RoM is simply shifted. The ThC3 and TrF angles in the front limbs (figure 3(Ci)), CTr angles in the middle limbs (figure 3(Bii)), and FTi angles in the front limbs (figure 3(Ciii)) follow this trend.

We additionally found that in cases where multiple DoF acted in the same plane, such as the levation/depression DoF, summing the angles of Scale-*Drosophila*'s multiple DoF produces a profile similar to that of the single DoF in Drosophibot II. To illustrate this point, the sum of the ThC2 and CTr angles of Scale-*Drosophila* is presented in black in figures 3(Aii), (Bii) and (Cii). For the middle and hind limbs (figures 3(Aii) and (Bii)), the combination of the ThC2 and CTr have trajectories and RoM more similar to Drosophibot II's CTr angles than Scale-*Drosophila*'s CTr angles alone.

To quantify the degree of similarity between each shared DoF, we applied a linear regression model to the two angle datasets and calculated the R-squared value for each common DoF between the two organisms (table S2). For the flat plane terrain, 10 of the 11 Drosophibot II DoF presented in figure 3 have a R-squared value greater than 0.8, six of which have values over 0.9. As the other tripod of legs will have the same joint angles time-shifted, this analysis shows that 20 of the 22 DoF on Drosophibot are kinematically similar to the animal when walking on a flat plane.

For the ball terrain, some DoF angles, particularly those in the hind and front legs, change from their flat plane values to accommodate moving at a vertical slope down the ball's surface (figure S6). However, the relationships between the Drosophibot II and Scale-*Drosophila* data established in the flat plane case persist; the main difference is which DoF follow which relationships. Some Drosophibot II DoF, like the front CTr (figure S6(Cii)) no longer have negligible difference from the fly model, but still have similar RoM and profile. Others, like the front ThC1 (figure S6(Ci)), become a closer match between the two organisms across most of the step. Table S3 shows the R-squared values for a linear regression of each common DoF while stepping on the ball terrain. In this case, eight of the 11 DoF have an R-squared value greater than 0.9. The remaining three DoF have a R-squared value of over 0.5. As such, 16 of the 22 DoF on Drosophibot are closely kinematically similar to the animal while walking on a ball.

The similarity of the majority of DoF across both the flat plane and ball terrains demonstrates the capability of our robot to produce fly-like movements in individual leg segments.

#### *3.1.2. Robot and fly dynamic comparison*

Figure 4 presents a qualitative comparison between Drosophibot II (solid lines) and Scale-*Drosophila* (dashed lines) of the torques required from each DoF over a single step across a flat plane to produce the kinematics presented in section 3.1.1 and figure 3. Figure S7 shows similar analysis for a ball terrain. Tables S4 and S6 present the R-squared values for linear regressions of the torque between each shared DoF in the robot and animal models. Unlike with the previous kinematic analysis, achieving closely

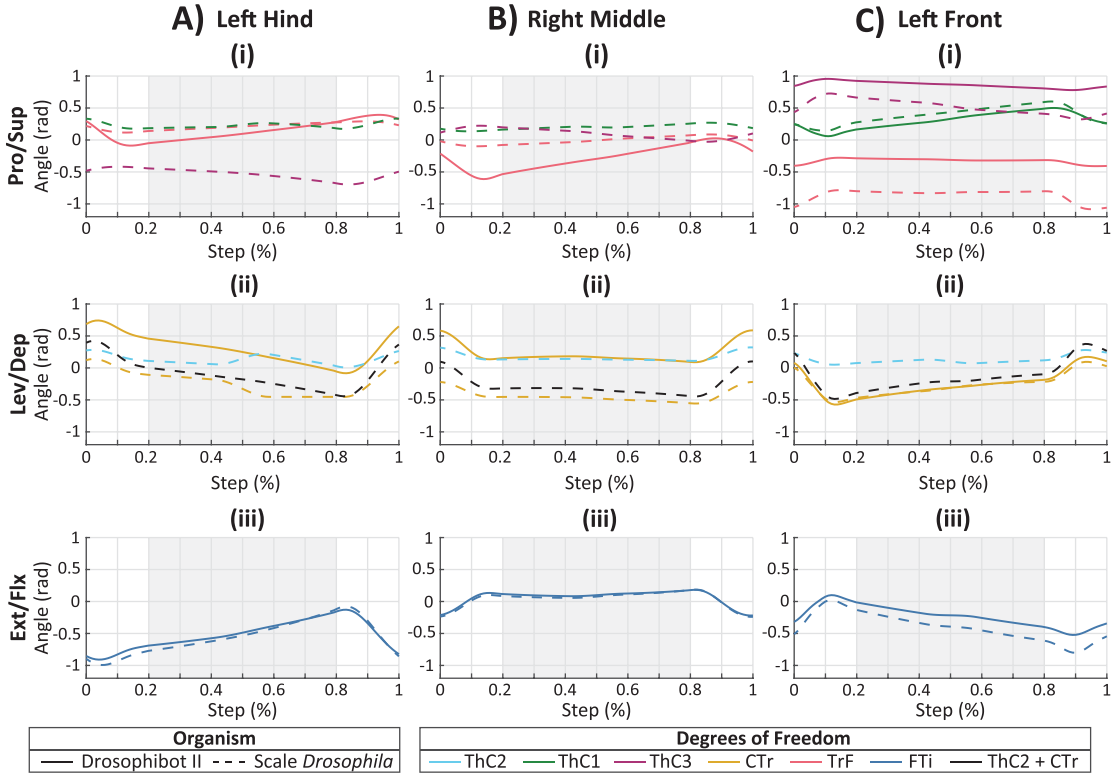


**Figure 3.** Modeled angles for each mobile DoF in the Drosophibot II (solid) and Scale-*Drosophila* (dashed) organism models throughout a step on a flat plane for a hind (Ai–iii), middle (Bi–iii), and front (Ci–iii) leg. DoF are grouped by the type of motion they provide in the leg: pronation/supination (Ai), (Bi) and (Ci), levation/depression (Aii), (Bii) and (Cii), and extension/flexion (Aiii), (Biii) and (Ciii). Grey shaded areas represent the stance phase of the leg. The sum of the ThC2 and CTr angles from the Scale-*Drosophila* model is additionally provided in black in (Aii), (Bii) and (Cii).

aligning torque magnitudes is infeasible. Rather, we are only interested in achieving similar torque trajectories across the step. This ensures that the robot will produce similar loading and unloading scenarios as the fly, which is useful for investigations of sensory feedback from the legs.

For each terrain, two different cases were considered; one in which no parallel stiffness was added to the joints (figures 4(A) and S7(A)), and one in which parallel elastic components were included (figures 4(B) and S7(B)). Elastic and viscous forces from the muscles and other tissues within the leg have been found to dominate motions in insects [1, 41], so analyzing these two cases allowed us to consider the effects of elasticity on both organisms' dynamics. We used a joint stiffness value of $k_{\text{joint}} = 3.8 \times 10^{-8}$ Nm rad$^{-1}$ for Scale-*Drosophila*, and a value of $k_{\text{joint}} = 1$ Nm rad$^{-1}$ for Drosophibot II. The value for *Drosophila* was calculated based on dynamic scaling calculations presented in [91]. The value for Drosophibot II was selected such that the resulting torques at each DoF would not overload our selected actuators and the stiffness was feasible to produce with physical components at the scale of the robot. The torques for Drosophibot II are presented in Nm, while the torques for Scale-*Drosophila* are in $\mu$Nmm.

Without parallel stiffness, Drosophibot II's DoF dynamics across both terrains follow similar trajectories as those of Scale-*Drosophila*. In this case, eight of the 11 DoF in this tripod have R-squared values over 0.9 while walking on either terrain (tables S4–5), meaning 16 Drosophibot II DoF have highly similar torque profiles to those of Scale-*Drosophila*, both on the flat plane (figure 4(A)) and on the ball (figure S7(A)). Including elastic elements in parallel with the joints (figures 4(B) and S7(B)) produces substantial effects on the torques required from each DoF. The largest magnitude torques now occur during swing instead of stance, as the most dominant force in the leg becomes the restoring moments from the elastic components. The force of supporting the body helps resist these moments, lowering the torque during the stance phase of the step. The inclusion of parallel elasticity also substantially increases the overall magnitude of the torques, particularly in scale-*Drosophila*; in some scale-*Drosophila* DoF, such as the FTi, the torques are close to double their values without parallel elasticity (figures 4(Avii, ix) and (Bvii, ix)). Due

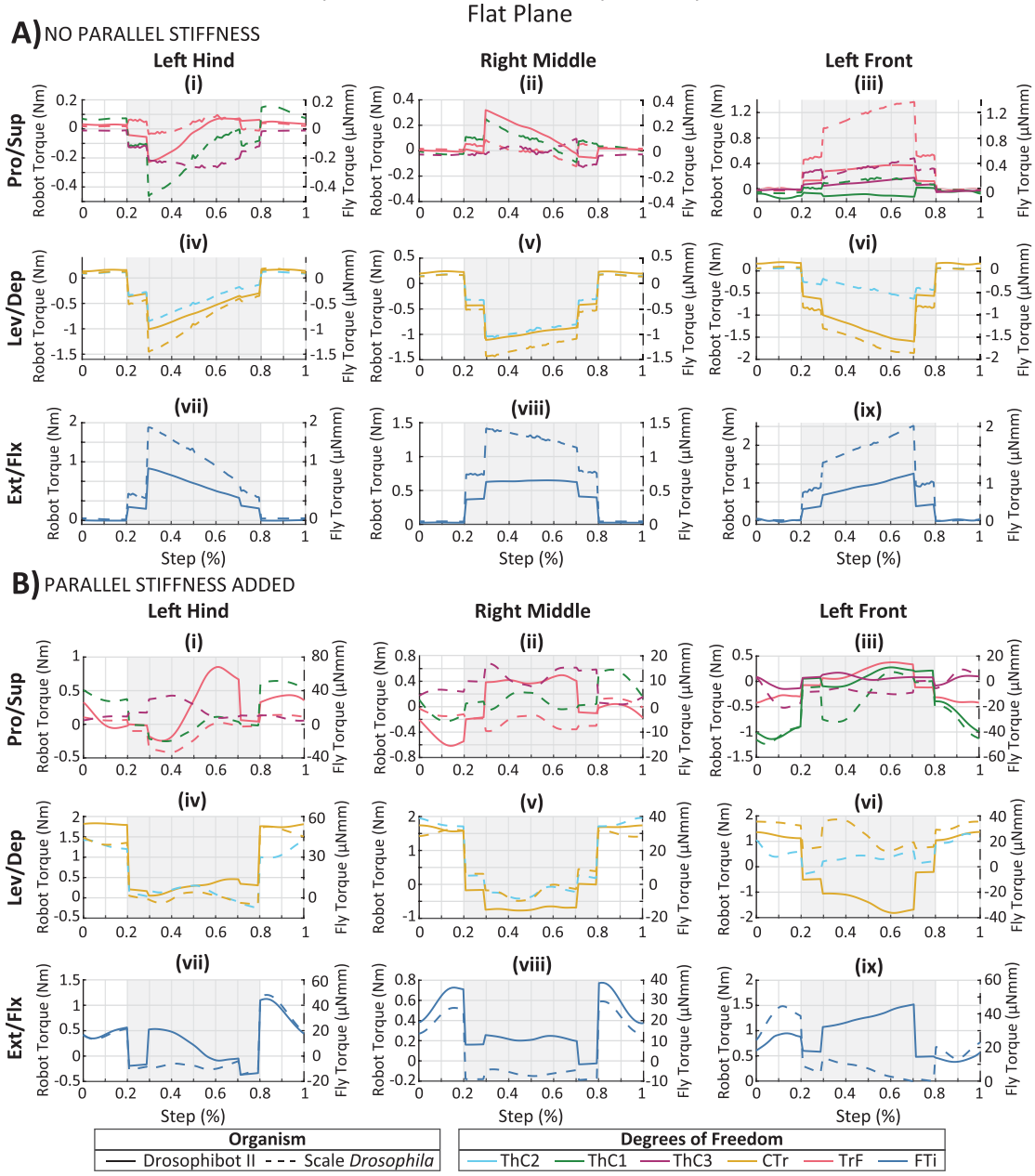


**Figure 4.** Modeled torques needed from each DoF in the hind (Ai, iv, vii; Bi, iv, vii), middle (Aii, v, viii; Bii, v, viii), and front (Aiii, vi, ix; Biii, vi, ix) Drosophibot II (solid) and Scale-*Drosophila* (dashed) organism models to complete a step on a flat plane with the kinematics presented in figure 3. Joints are grouped by the type of motion they broadly provide in the leg. Grey shaded areas represent the stance phase of the leg. (A) Comparison with no parallel stiffness added to the joints. (B) Comparison with a parallel stiffness of 1 Nm rad$^{-1}$ in Drosophibot II and $3.8 \times 10^{-8}$ Nm rad$^{-1}$ in Scale-*Drosophila*.

to the overall higher torque magnification in scale-*Drosophila*, the R-squared values for linear regression models between the two organisms are lower than prior cases. However, most of the trajectories of shared DoF remain similar across both terrains. In the flat plane case, five of the 11 common DoF in figure 4 have R-squared values greater than 0.7, with six total having a value over 0.5 (table S4). For the ball terrain, five common DoF have R-squared values over 0.5 (table S6). These values quantitatively show that at least 10 of 22 DoF on the robot are dynamically similar to those in the fly for both terrains when parallel elasticity is included.

### *3.1.3. Fly walking terrain comparisons*

We also used our Scale-*Drosophila* model to compare the kinematics and dynamics of the animal while walking on a flat plane versus a ball. Current setups for recordings of neural activity and 3D motion capture during *Drosophila* walking primarily utilize a

ball treadmill [6, 51, 52, 83], but we plan to run the robot on terrains more closely resembling flat planes. As such, comparing the two terrains in simulation enables us to investigate the effects of these terrains on fly walking and their overall similarity. This comparison was conducted for walking trials with a step period of 0.275 s, walking parameters outlined in table 1, and joint stiffness of $3.8 \times 10^{-8}$ Nm rad$^{-1}$.

Figure S8 qualitatively compares the angles and torques for each DoF in a hind, middle, and front leg of Scale-*Drosophila* during walking on the flat plane (solid) and ball (dashed) terrains. Tables S7 and S8 provide R-squared values from linear regressions of each DoF across terrains for the kinematics and dynamics, respectively. In the hind and middle legs (figures S8(A) and (B)), each pair of DoF angles follow a highly similar trajectory over the step, with phasic differences of less than 0.2 rad. This is reflected in the R-squared values, with 16 of the 18 DoF with values greater than 0.7 (table S7). The smallest R-squared values occur in the proximal DoF of the hind legs, corresponding to the much steeper effective terrain angle the legs must traverse on the ball during stance.

The DoF torques are also quite similar. The largest discrepancies are in the front legs (figure S8(C)), where each DoF has larger, more consistent differences between the two terrains across the step. The magnitudes of these differences reach up to 0.5 rad, such as in the FTi joint. These larger discrepancies produce changes in the torques over the step, with magnitudes of up to 50 $\mu$Nmm. However, the trajectories of the angles and torques over the step remain similar; the R-squared values for the torques in each DoF across terrains are all greater than 0.7, with 11 of 18 greater than 0.9.

Figure S9 compares the GRFs in three legs of Scale-*Drosophila* during walking on the two different terrains. Each component of the GRF is plotted separately (figures S9(A)–(C)), as well as the total magnitude of the force vector (figure S9(D)). The GRF magnitudes on the ball are consistently higher than those for the flat plane, sometimes reaching close to double. This difference is most noticeable in the front legs (figure S9(D), right). However, both magnitudes are still within a similar range to magnitudes collected in the animal [106] and other *Drosophila* simulations [52].

Overall, our model of *Drosophila* exhibits similar DoF angles across a step for the flat plane and ball terrains. The resulting GRF magnitudes do differ substantially between the two terrains, but the short lengths of *Drosophila*'s leg segments and the alignment of its joint axes relative to gravity mean these external forces still produce similar internal torques. This means that data taken from the robot, which has been established as kinematically and dynamically similar to the fly for both terrains in sections 3.1.1 and 3.1.2, can be broadly compared to biological data collected on both surfaces.

### 3.2. Physical robot experiments

Videos S1–S3 show the robot walking forward, backward, and on an incline, respectively. These scenarios were selected based on biological experiments and datasets of interest in the animal. The following sections discuss the robot's performance during these experiments in greater detail.

#### *3.2.1. Effects of mass distribution*

Non-biological distribution of mass is a common critique of biomimetic robots such a Drosophibot II, as increased mass in the legs could result in substantially different moments of inertia, affecting walking dynamics [41]. To address these concerns, we modeled the inverse dynamics of the robot in our solver, and ran tests with the physical robot, for forward walking with multiple stepping periods and observed how the joint torques changed with stepping period. Figure 5 shows the modeled torques for each DoF in Drosophibot II, as well as the mean estimated torques from the robot's actuators over ten steps, for a hind (figures 5(A) and (B)), middle (figures 5(C) and (D)), and front (figures 5(E) and (F)) leg at stepping periods of 1 s (solid), 2 s (dashed), and 4 s (dotted). Video S1 shows an example of Drosophibot II walking forward with a step period of 2 s for 10 steps.

In simulation, decreasing the stepping period from 4 s to 2 s minimally affected the mean torques in each DoF (figures 5(A), (C) and (E)). Changes in torque became most pronounced when decreasing to 1 s steps, particularly in the swing phase of the front limbs, where torques increase by as much as 0.4 Nm (figure 5(E)). These dramatic increases are primarily during swing in the most proximal DoF, which must accelerate the full mass of the legs during this time.

As seen in the model, actuation torque in the proximal leg joints increases with stepping frequency in the physical robot data (figures 5(B), (D) and (F)). While there is some slight deviation between the 4 s and 2 s stepping, the overall magnitude and phasing of the mean torques remains similar across all DoF. The greatest change occurs when the stepping period is decreased to 1 s. This change most consistently results in a phase-lag of 0.1–0.175 s compared to the 2 s and 4 s torques. There are additional effects on the mean torque magnitudes, but these effects are inconsistent between DoF. Some DoF experience an increase in the mean torque (figure 5(Di)), others experience a decrease (figure 5(Bii)), and still others are roughly unchanged (figure 5(Fi)). However, in most DoF this change in magnitude, if any, is within the range of variance between the steps (shaded regions) used to form the mean value. The minimal changes in torque between the 4 s and 2 s cases in both the model and the physical robot demonstrates it is quasi-static in that

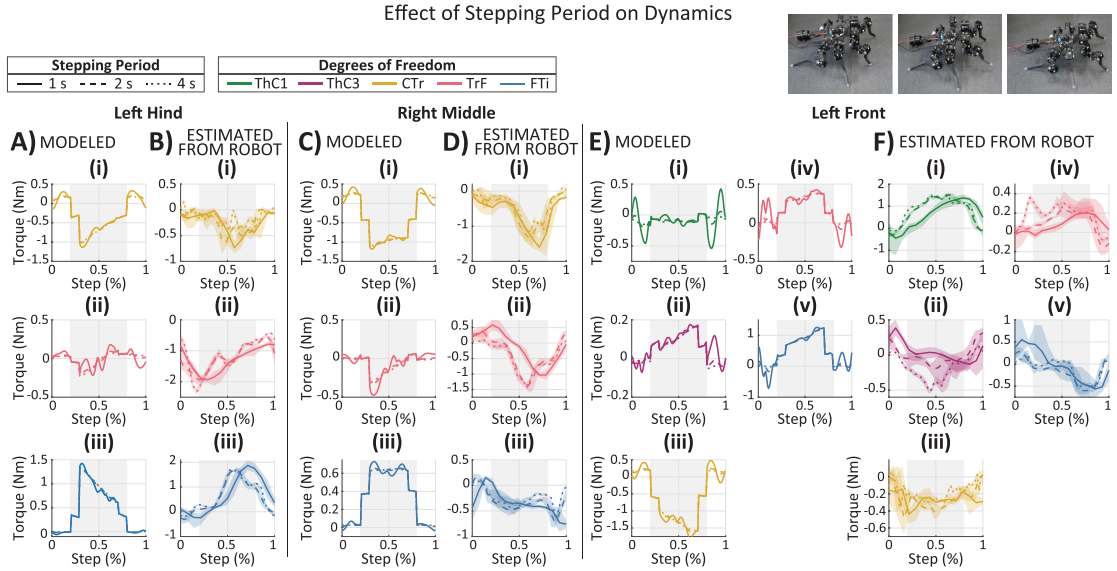


**Figure 5.** Joint torques for each joint in a hind (A)–(B), middle (C)–(D), and front (E)–(F) leg of Drosophibot II for stepping periods of 1 s (solid), 2 s (dashed), and 4 s (dotted). Torques were both modeled in our solver (A), (C), (E) and estimated from current readings from the physical robot's servos (B), (D), (F). Stepping data from the physical robot was averaged over five steps to generate a 'typical' step. Grey shaded areas represent the stance phase of the leg.

range of speeds, because if it were dominated by inertia, doubling the frequency in this way would quadruple the actuation torque. As such, we slowed the robot's behavior to minimize the effects of the non-biological distribution of mass on the dynamics of the robot in those range of walking speeds. Decreasing the stepping period to 1 s begins to shift the robot into a more inertially-dominated regime, providing a functional upper limit of walking speed for our experiments. These experiments also highlight the ability of the solver to predict aspects of the physical robot.

### *3.2.2. Backward walking*

We also used the physical robot to test how walking direction affects the dynamics in each DoF. Recent studies in *Drosophila* have identified brain neurons involved in the initiation of backwards walking, termed 'moonwalker' neurons [8, 27]. Backward walking in Drosophibot II is then useful to further explore the control regime involving these neurons. Figure 6 compares the torques for each DoF averaged over ten steps for one of each leg during forward (dashed) and backward (solid) walking at a 2 s stepping period. Video S2 shows an example of Drosophibot II walking backward for 10 steps. To generate backward walking, the kinematics from forward walking were run in reverse. As such, $Tr_{\text{body}} = -0.085$ m. No other stepping parameters were modified, and are given in table 1.

Reversing the walking direction changes the polarity and magnitude of several DoF's torques in each leg pair. Which DoF are most affected varies across leg pairs. In the hind legs, walking backward increases the torque requirements of the TrF (figure 6(Aii)) and reverses the torque directions throughout the trajectory of the FTi (figure 6(Aiii)). In the middle legs, the magnitudes of the CTr (figure 6(Bi)) and the TrF (figure 6(Bii)) torques are decreased during stance, and the slopes are reversed such that the values approach zero or become positive, respectively, rather than remaining negative. The front leg ThC1 (figure 6(Ci)) and FTi (figure 6(Cv)) undergo significant changes in magnitude during stance. Additionally, the trajectories of the front leg CTr (figure 6(Ciii)) and ThC3 (figure 6(Cii)) change from concave-up to concave-down. Of the 22 DoF in Drosophibot, 14 experience significant changes to their magnitude or polarity when walking backward. However, these changed values are still within the capabilities of the actuators, and the robot is able to walk in either direction without issue. This result also suggests that the dynamics of backward walking change in non-trivial ways. For example, roles of the front and hind legs reverse, with the front legs accelerating the body and the hind legs now decelerating the body [28]. This may have greater implications for the nuance of backward walking control.

### *3.2.3. Incline walking*

Finally, we tested the robot's capability to walk on an inclined surface and recorded how the torques in each DoF changed from baseline flat-ground walking. Several studies have explored how sensory feedback and nervous system control may change for incline walking in insects (e.g. [20, 108]), making incline walking in Drosophibot II valuable for further exploration. Figure 7 compares the torques for each DoF averaged over five steps for a hind, middle, and front leg during walking up a 15° ramp (solid) and a flat plane over ten steps (dashed). Video S3

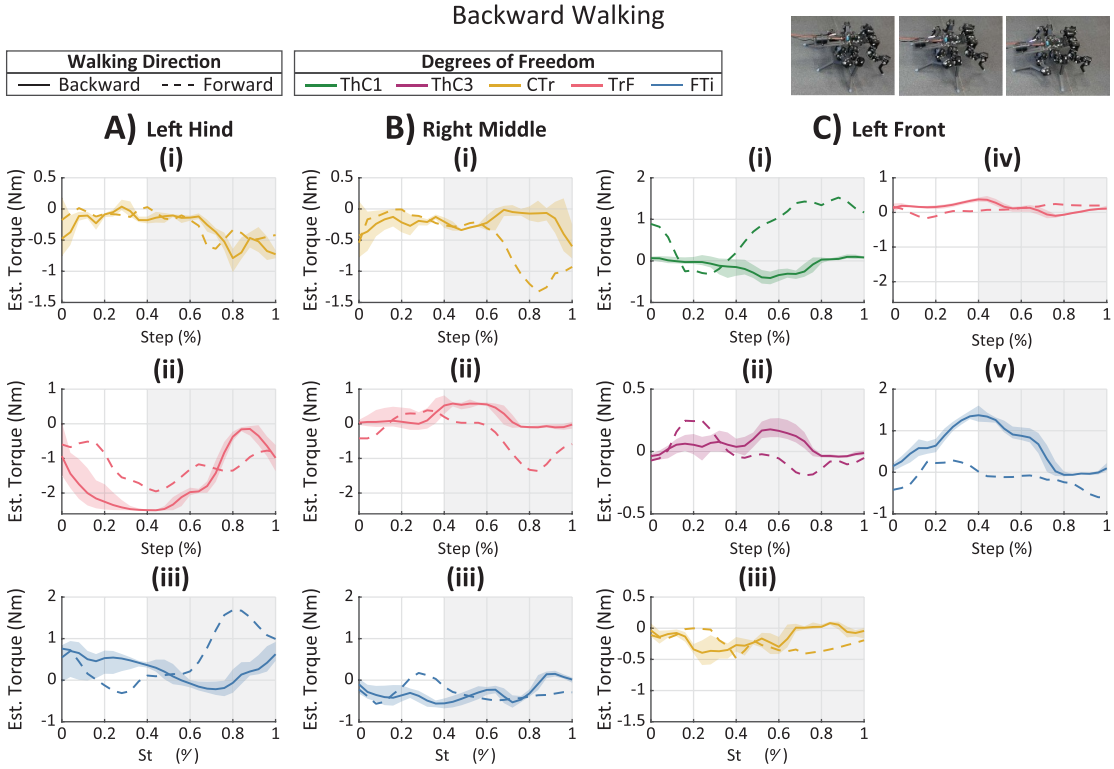


**Figure 6.** Comparison of joint torques estimated using current draw from each joint's actuator in a hind (A), middle (B), and front (C) leg of Drosophibot II during forward (dashed) and backward (solid) walking at a 2 s stepping period. To generate backward walking, kinematics from forward walking were run in reverse. Grey shaded areas represent the stance phase of the leg.

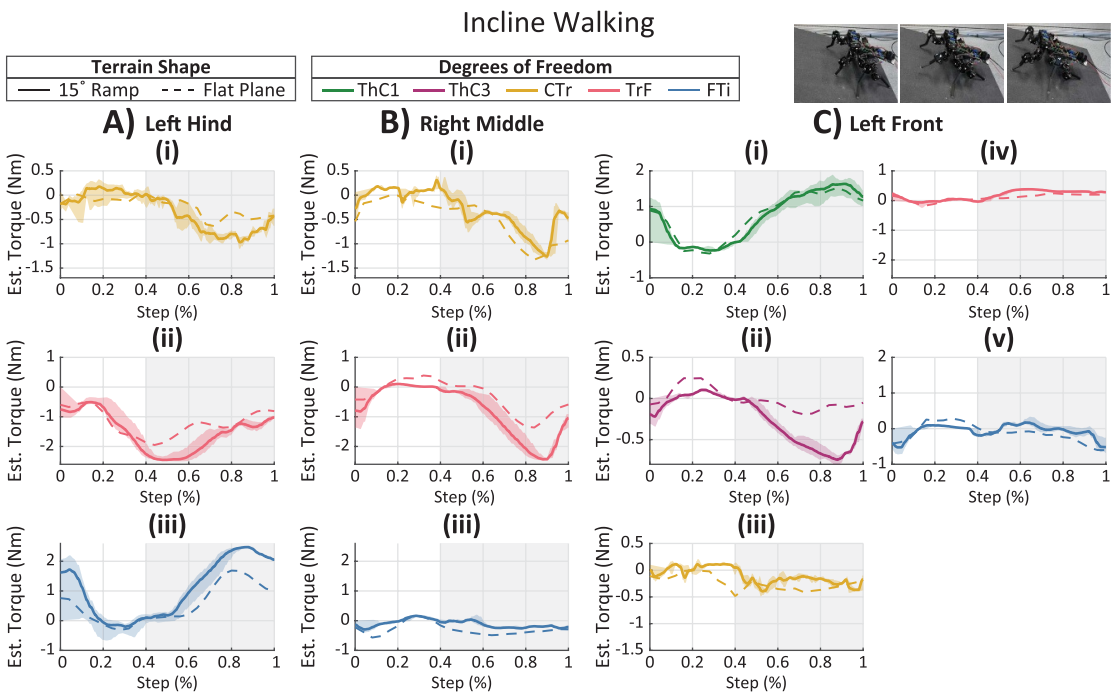


**Figure 7.** Joint torques estimated using current draw from each joint's actuator in a hind (A), middle (B), and front (C) leg of Drosophibot II during incline (solid) and flat plane walking at a 2 s stepping period. Grey shaded areas represent the stance phase of the leg.

shows an example of Drosophibot II walking up an incline for 5 steps. Overall, the torques required in DoF providing pronation/supination of the legs (TrF in the middle and hind legs, figures 7(Aii) and (Bii); TrF and ThC3 in the front legs, figures 7(Cii, iv)) during stance greatly increased while walking up the incline. The hind FTi torque showed similar increase (figure 7(Aiii)). In these cases, the torques neared, but

did not reach, the stall torques of the motors, and the robot was still able to climb to the top of the ramp by the end of the trial.

## 4. Discussion and conclusion

The development and experimental validation of Drosophibot II, a biomimetic robot modeled after an adult fruit fly, is presented (figure 1). The robot was designed with close consideration of leg proportions and necessary DoF informed by walking kinematic data from the animals. Its mechatronics were designed using a program that calculates the inverse kinematics for biomimetic walking and solves the inverse dynamics throughout a single step (figure 2). Using this solver program, Drosophibot II was compared to a scale model of *Drosophila*. The solver demonstrates that the two organisms produce similar motions in their leg segments while stepping through the same footpaths on both a flat plane and a ball; the majority of robot DoF either had similar trajectories and ranges of motion to shared insect DoF, or to the sum of all insect DoF acting within the same plane (figures 3 and S6). Dynamically, the majority of modeled torques for each robot DoF had similar trajectories to those of the insect in cases with and without insect-like parallel elasticity in the joints (figures 4 and S7). In the physical robot, actuator torques were found to be similar across three different stepping periods, demonstrating that Drosophibot II is quasi-static for our intended walking speeds (figure 5). The robot was able to execute straight-line forward and backward walking on a flat plane using the joint angles generated by our solver (figure 6), as well as forward walking on an incline (figure 7).

### 4.1. Flat plane vs. ball walking

It is presently an open question how similar *Drosophila*'s walking is across a flat plane and a ball (for a preprint, see [68]). Current ball treadmill setups allow for 3D joint tracking [38], as well as straightforward determination of walking direction. However, the terrain itself is not naturalistic, motivating the use of a flat plane. Tethered flat plane treadmills have a variety of technical constraints such as difficulty minimizing friction, and recording 3D leg kinematics of freely walking flies at the joint level in current experimental setups (i.e. petri dishes, glass plates) is prohibitively difficult. By modeling both terrain shapes in our solver, we were able to explore how fly mechanics across these two terrain shapes may differ. Kinematically, we found that DoF angles were minimally affected; while some DoF differed on the ball relative to the flat plane angles across the step, these differences were phasic and less than 0.2 rad in magnitude. Dynamically, we found that while GRFs may be significantly larger during ball walking, the torques required at each DoF were minimally affected. This minimal torque difference is likely due to the very small moment arms produced by *Drosophila*'s leg segments decreasing the affect of force increases on the overall torque values.

Currently our calculated GRFs and joint torques for the fly are on the same order of magnitude as both biological force data collected from *Drosophila* jumping [106] and calculated values from other simulation frameworks such as NeuroMechFly [52]. However, detailed GRFs during walking are not presently available from the animal. As biological data collection setups continue to advance, we will be able to compare our solved values to additional force measurements.

### 4.2. Future areas of interest

Completing mechatronic development of Drosophibot II enables a host of potential applications to neuromechanical research. Our primary areas of interest in this regard are detailed below.

#### *4.2.1. Nervous system-based walking controllers*

The robot can be used as a test platform for nervous system-inspired walking controllers, also called SNSs [31, 64, 75, 96], such as the one previously developed for the first Drosophibot [32]. By modeling the dynamics of neurons and synapses, as well as the morphology of the nervous system, these controllers can increase our understanding of how the nervous system controls legged locomotion and motor control in general. For example, many recent studies focused on how descending control contributes to the initiation, maintenance, and task-specific modulation of locomotive behaviors in *Drosophila*, leading to identification of brain neurons involved in forward walking, turning, and backwards walking [7, 8, 27]. In this context, Drosophibot II can serve to test diverse putative descending control regimes based on data from neurobiological studies.

#### *4.2.2. Leg coordination during stepping*

Drosophibot II can also be used to further investigate how leg coordination patterns contribute to a variety of walking behaviors. Biological and simulation studies have previously investigated how interleg coordination varies during behaviors such as stepping on uneven terrains [11, 63], walking at different speeds [92, 105], and walking in a curve [84, 93] in flies and arthropods. SNS walking controllers could be used on Drosophibot II to explore how the fly's nervous system controls these different walking regimes in detail. Additionally, while only tripod coordination patterns are presented in the present work, our solver can generate coordination schemes with arbitrary ipsilateral and contralateral phase differences between legs. Thus, the robot could be controlled through solver kinematic replay across a wide array of leg coordination patterns for studies more focused on the mechanics of walking (e.g. ease of traversal for different gaits across rough substrates).

*4.2.3. Joint parallel elasticity*

Our inverse dynamic torque data for the robot and fly body-plans highlights the importance of considering joint elasticity in biomimetic platforms. Adding insect-like parallel elasticity to our model significantly changed the torque magnitudes and trajectories for each part of a step in every DoF by producing elastic restoring moments. In other studies, such elastic components have been found to require different control mechanisms than those for inertially-dominated organisms, such as consistent motor-neuron activation during swing phase [1, 42], and 'braking' forces from opposing muscles to tune/halt rapid passive restoring moments [74]. Several robotic studies have also highlighted how parallel elasticity can aid in generating movement torques in underactuated systems [58], improve robustness to sensorimotor delays [4], and store elastic energy for later rapid release [44]. *Drosophila*'s nervous system has evolved to control body mechanics more resembling our model with parallel elasticity than the model without, so including parallel elastic components on Drosophibot II will be important for future endeavors into matching the mechanical and neural dynamics of biomimetic walking, as well as further exploring the benefits parallel elasticity can provide to meso-scale robots comparable to Drosophibot II. Initial work will likely involve modular components with a set stiffness value mounted external to the actuators, though the recent increasing focus on developing compact parallel elastic actuators with tuneable stiffness [36, 49, 67] could eventually spur a redesign of Drosophibot II with new actuators.

*4.2.4. Biomimetic sensory feedback*

The robot can also serve as a data-collection platform for biomimetic sensory feedback. Several studies have previously used biologically-inspired robots to investigate sensory discharge from CS, mechanoreceptors on the insect exoskeleton that encode strain [24, 32, 33, 111]. These studies primarily focus on single-leg stepping. By including strain gauges in biological locations on Drosophibot II's limbs, strain data that may be available to the nervous system throughout six legged stepping can be hypothesized. To this end, it is beneficial that the torque trajectories modeled for the CTr and FTi in each leg were minimally affected by changing the body plan; the CTr and FTi torques in Drosophibot II were similar to those in scale-*Drosophila* even with other DoF removed, implying the strains in these segments may also be similar. The roles of CS fields on the trochanter and tibia have been investigated for many years in a variety of insects [22, 107, 109, 110], but recording from many sensilla in a walking animal is prohibitively difficult. Recording strain data from these locations on Drosophibot II will contribute to this body of work by producing strain readings from all CS locations on all legs at once that are functionally comparable to the animal. Because the robot can traverse inclines as well as flat ground, we can conduct experiments like those carried out in animals such as the stick insect to observe the effects on biological limb strain [20, 108].

Additionally, we have used our *Drosophila*-scale body plan to generate theoretical values for animal-like GRFs and reaction forces and moments at each joint, which could be of particular interest for calculating biologically plausible limb stresses and strains for finite element analysis of the insect cuticle [22]. Such simulations improve our understanding of what stresses and strains are experienced during locomotion, and how they activate CS across the leg.

### 4.3. Limitations

Though we have carefully considered the kinematics and dynamics of Drosophibot II in order to match them to *Drosophila*, the present study has limitations. First, although the leg segment lengths of the robot are closely proportional to the animal's, the distances between the ThC joints (or where the ThC would be, in the case of the middle and hind legs) have significantly more error due to the size of the actuators. The actuators in Drosophibot II were positioned as close as possible to each other both laterally and along the body such that the distances between leg pairs were still proportional. For example, the lateral distance between the middle leg pair ThC joints was lengthened to the minimum distance possible without the CTr servos colliding, then the lateral distances between the front and hind limbs were also extended to keep the distances between the ThC pairs scaled biomimetically. However, the relative size of the actuators still produced thorax dimensions up to $\times 10$ greater than those in the fly. Our solver produces footpaths based on the location of each leg's ThC in the global frame, so we do not believe these increased thorax dimensions significantly affect the kinematics and dynamics between our modeled organisms. In the future, the legs could be positioned closer together by moving the actuators into the body and using belts or cables to drive the joints [5, 50, 69].

Additionally, our inverse dynamic solver makes simplifications that could affect the model's accuracy to the physical robot's dynamics. Our solver does not include difficult-to-simulate parameters such as slip between the foot and substrate and elastic deformation of the 3D printed materials, which can cause sagging of the robot posture. External torques on the servos can also cause the robot posture to sag because the servo produces torque using a proportional feedback controller in which the output torque equals the positional error multiplied by a proportional gain term. A variety of methods exist to model these parameters in detail but our established goal was to use the solver to develop a physical robot rather than create a perfect simulation. As such, we chose to address these parameters on the physical platform rather than

devoting the time to completely modeling their behavior. We attempt to alleviate differences between the model and the robot by first offsetting the body height for each leg pair in the solver when generating kinematics for running the physical robot, such that the sagging due to material deformation and the offset would counteract each other. In addition, we bias the servo angle commands by the torque modeled in the solver divided by the spring coefficient of the actuator. This term is equivalent to the inverse of that used in the proportional feedback controller of the servo. Although we did not carefully quantify how these solutions changed the robot's posture, it was anecdotally observed to improve the body height during testing. The solver also does not account for accelerations of the main body segment, which naturally occurs as the animal's thorax bobs or rotates during walking. On the physical robot, the thorax CoM will naturally shift slightly as different leg combinations enter and leave stance.

It is presently difficult to quantitatively determine how these simplifications affect our model's accuracy, as the robot actuators' 'torque' readings are extrapolated from the current draw of the motor. While the manufacturer provides conversions for these readings, they have been found to have idiosyncratic inaccuracy in bench-top experiments. As such, the readings are primarily useful only for comparing robot data to other robot data. Future work will involve both attempting to minimize the effect of these unmodeled forces (e.g. increasing the coefficient of friction between the tarsi tips and the ground) and exploring alternate ways to read accurate actuator torque data from the robot.

### 4.4. Conclusion and final thoughts

In this work we designed, built, and validated Drosophibot II, a kinematically- and dynamically-scaled robotic model of the fruit fly. The robot's kinematics are based on 3D point tracking data, while its dynamics are validated to be quasi-static like an insect. The robot is capable of performing behaviors studied in literature, including forward and backward walking, as well as walking up an incline. We plan to use this robot to better understand the mechanics, motor control, and sensory processing of the fruit fly and other insects by recording sensory feedback and experimenting with models of nervous system motor control. Such understanding can be used to uncover overarching principles in the nervous system for general robust locomotion, which can be applied to other organisms as well as walking robots.

## Data availability statement

All data that support the findings of this study are included within the article (and any supplementary files).

## Funding

This work was supported by the National Science Foundation (NSF 2015 317 to NSS) and the Deutsche Forschungsgemeinschaft (DFG Bu857/15 and BL1355/6-1 [43 625 8345] to AB) as part of the International Next Generation Network for Neuroscience (NeuroNex) Program.

MH and AB are members of the 'iBehave' network funded by the Ministry of Culture and Science of the State of North Rhine-Westphalia.

## ORCID iDs

Clarus A Goldsmith https://orcid.org/0000-0002-3193-520X
Moritz Haustein https://orcid.org/0000-0003-4493-6161
Ansgar Büschges https://orcid.org/0000-0003-2123-1900
Nicholas S Szczecinski https://orcid.org/0000-0002-6453-6475

## References

[1] Ache J M and Matheson T 2013 Passive joint forces are tuned to limb use in insects and drive movements without motor activity *Curr. Biol.* **23** 1418–26
[2] Agrawal S, Dickinson E S, Sustar A, Gurung P, Shepherd D, Truman J W and Tuthill J C 2020 Central processing of leg proprioception in *Drosophila eLife* **9** 1–32
[3] Aronhalt E, Abramson E, Goldsmith C A, Andrada E, Nourse W, Sutton G, Szczecinski N S and Quinn R D 2023 Development of a robotic rat hindlimb model *Biomimetic and Biohybrid Systems* ed F Meder, A Hunt, L Margheri, A Mura and B Mazzolai (Springer International Publishing) pp 115–30
[4] Ashtiani M S, Sarvestani A A and Badri-Spröwitz A 2021 Hybrid parallel compliance allows robots to operate with sensorimotor delays and low control frequencies *Front. Robot. AI* **8** 645748
[5] Badri-Spröwitz A, Aghamaleki Sarvestani A, Sitti M and Daley M A 2022 BirdBot achieves energy-efficient gait with minimal control using avian-inspired leg clutching *Sci. Robot.* **7** eabg4055
[6] Berendes V, Zill S N, Büschges A and Bockemühl T 2016 Speed-dependent interplay between local pattern-generating activity and sensory signals during walking in *Drosophila J. Exp. Biol.* **219** 3781–93
[7] Bidaye S S, Laturney M, Chang A K, Liu Y, Bockemühl T, Büschges A and Scott K 2020 Two brain pathways initiate distinct forward walking programs in *Drosophila Neuron* **108** 469–485.e8
[8] Bidaye S S, Machacek C, Wu Y and Dickson B J 2014 Neuronal control of *Drosophila* walking direction *Science* **344** 97–101
[9] Billeschou P, Bijma N N, Larsen L B, Gorb S N, Larsen J C and Manoonpong P 2020 Framework for developing bio-inspired morphologies for walking robots *Appl. Sci.* **10** 1–20
[10] Brand A H and Perrimon N 1993 Targeted gene expression as a means of altering cell fates and generating dominant phenotypes *Development* **118** 401–15
[11] Brandt E E, Manyama M R and Nirody J A 2024 Kinematics and coordination of moth flies walking on smooth and rough surfaces *Ann. New York Acad. Sci.* **1537** 64–73

[12] Brooks R A 1989 A robot that walks: emergent behaviors from a carefully evolved network *IEEE Int. Conf. on Robotics and Automation* vol 2 pp 692–704
[13] Bujard T, Giorgio-Serchi F and Weymouth G D 2021 A resonant squid-inspired robot unlocks biological propulsive efficiency *Sci. Robot.* **6** eabd2971
[14] Buschmann T, Ewald A, von Twickel A and Büschges A 2015 Controlling legs for locomotion-insights from robotics and neurobiology *Bioinspir. Biomim.* **10** 41001
[15] Büschges A, Scholz H and El Manira A 2011 New moves in motor control *Curr. Biol.* **21** R513–24
[16] Chockley A S, Dinges G F, Di Cristina G, Ratican S, Bockemühl T and Büschges A 2022 Subsets of leg proprioceptors influence leg kinematics but not interleg coordination in *Drosophila melanogaster* walking *J. Exp. Biol.* **225** jeb244245
[17] Cofer D, Cymbalyuk G, Reid J, Zhu Y, Heitler W J and Edwards D H 2010 AnimatLab: a 3D graphics environment for neuromechanical simulations *J. Neurosci. Methods* **187** 280–8
[18] Cruse H 1990 What mechanisms coordinate leg movement in walking arthropods? *Trends Neurosci.* **13** 15–21
[19] Cruse H and Schwarze W 1988 Mechanisms of coupling between the ipsilateral legs of a walking insect (*Carausius Morosus*) *J. Exp. Biol.* **138** 455–69
[20] Dallmann C J, Dürr V and Schmitz J 2019 Motor control of an insect leg during level and incline walking *J. Exp. Biol.* **222** jeb188748
[21] de Croon G 2020 Flapping wing drones show off their skills *Sci. Robot.* **5** eabd0233
[22] Dinges G F, Bockemühl T, Iacoviello F, Shearing P R, Büschges A and Blanke A 2022 Ultra high-resolution biomechanics suggest that substructures within insect mechanosensors decisively affect their sensitivity *J. R. Soc. Interface* **19** 20220102
[23] Dinges G F, Chockley A S, Bockemühl T, Ito K, Blanke A and Büschges A 2021 Location and arrangement of campaniform sensilla in *Drosophila melanogaster J. Comp. Neurol.* **529** 905–25
[24] Dinges G F, Zyhowski W P, Goldsmith C A and Szczecinski N S 2023 Comparison of proximal leg strain in locomotor model organisms using robotic legs *Biomimetic and Biohybrid Systems* ed F Meder, A Hunt, L Margheri, A Mura and B Mazzolai (Springer International Publishing) pp 411–27
[25] Dürr V *et al* 2019 Integrative biomimetics of autonomous hexapedal locomotion *Front. Neurorobot.* **13** 1–32
[26] Espenschied K S, Quinn R D, Beer R D and Chiel H J 1996 Biologically based distributed control and local reflexes improve rough terrain locomotion in a hexapod robot *Robot. Auton. Syst.* **18** 59–64
[27] Feng K, Sen R, Minegishi R, Dübbert M, Bockemühl T, Büschges A and Dickson B J 2020 Distributed control of motor circuits for backward walking in *Drosophila Nat. Commun.* **11** 6166
[28] Full R J, Blickhan R and Ting L H 1991 Leg design in hexapedal runners *J. Exp. Biol.* **158** 369–90
[29] Full R J and Koditschek D E 1999 Templates and anchors: neuromechanical hypotheses of legged locomotion on land *J. Exp. Biol.* **202** 3325–32
[30] Goldsmith C A, Haustein M, Bockemühl T, Büschges A and Szczecinski N S 2022 Analyzing 3D limb kinematics of *Drosophila melanogaster* for robotic platform development *Biomimetic and Biohybrid Systems* ed A Hunt, V Vouloutsi, K Moses, R Quinn, A Mura, T Prescott and P F M J Verschure (Springer International Publishing) pp 111–22
[31] Goldsmith C A, Quinn R D and Szczecinski N S 2021 Investigating the role of low level reinforcement reflex loops in insect locomotion *Bioinspir. Biomim.* **16** 065008
[32] Goldsmith C A, Szczecinski N S and Quinn R D 2020 Neurodynamic modeling of the fruit fly *Drosophila melanogaster Bioinspir. Biomim.* **15** 065003
[33] Goldsmith C A, Zyhowski W P, Büschges A, Zill S N, Dinges G F and Szczecinski N S 2023 Effects of tarsal morphology on load feedback during stepping of a robotic stick insect (*Carausius morosus*) limb *Biomimetic and Biohybrid Systems* ed F Meder, A Hunt, L Margheri, A Mura and B Mazzolai (Springer International Publishing) pp 442–57
[34] Graziane N and Dong Y 2022 *Electrophysiological Analysis of Synaptic Transmission* vol 187 (Springer) ch 1, pp 3–15
[35] Günel S, Rhodin H, Morales D, Campagnolo J, Ramdya P and Fua P 2019 DeepFly3D, a deep learning-based approach for 3D limb and appendage tracking in tethered, adult *Drosophila eLife* **8** 1–23
[36] Hajj-Ahmad A, Kyungwon Han A, Lin M A, Glover G H and Cutkosky M R 2023 An electrostatically actuated gecko adhesive clutch *Adv. Mater. Technol.* **8** 2202025
[37] Hales K G, Korey C A, Larracuente A M and Roberts D M 2015 Genetics on the fly: a primer on the *Drosophila* model system *Genetics* **201** 815–42
[38] Haustein M, Blanke A, Bockemühl T and Büschges A 2024 A leg model based on anatomical landmarks to study 3D joint kinematics of walking in *Drosophila melanogaster Front. Bioeng. Biotechnol.* **12** 1357598
[39] Hermans L, Kaynak M, Braun J, Ríos V L, Chen C L, Friedberg A, Günel S, Aymanns F, Sakar M S and Ramdya P 2022 Microengineered devices enable long-term imaging of the ventral nerve cord in behaving adult *Drosophila Nat. Commun.* **13** 1–15
[40] Holmes P, Full R J, Koditschek D and Guckenheimer J 2006 The dynamics of legged locomotion: models, analyses and challenges *SIAM Rev.* **48** 207–304
[41] Hooper S L 2012 Body size and the neural control of movement *Curr. Biol.* **22** R318–22
[42] Hooper S L, Guschlbauer C, Blümel M, Rosenbaum P, Gruhn M, Akay T and Büschges A 2009 Neural control of unloaded leg posture and of leg swing in stick insect, cockroach and mouse differs from that in larger animals *J. Neurosci.* **29** 4109–19
[43] Hutter M *et al* 2016 ANYmal—a highly mobile and dynamic quadrupedal robot *IEEE Int. Conf. on Intelligent Robots and Systems* vol 2016-Novem pp 38–44
[44] Hyun N P, Olberding J P, De A, Divi S, Liang X, Thomas E, St. Pierre R, Steinhardt E, Jorge J and Longo S J 2023 Spring and latch dynamics can act as control pathways in ultrafast systems *Bioinsp. Biomim.* **18** 026002
[45] Ijspeert A J 2014 Biorobotics: using robots to emulate and investigate agile locomotion *Science* **346** 196–203
[46] Ijspeert A J, Crespi A, Ryczko D and Cabelguen J-M 2007 From swimming to walking with a salamander robot driven by a spinal cord model *Science* **315** 1416–20
[47] Ji A, Zhao Z, Manoonpong P, Wang W, Chen G and Dai Z 2018 A bio-inspired climbing robot with flexible pads and claws *J. Bionic Eng.* **15** 368–78
[48] Karakasiliotis K, Thandiackal R, Melo K, Horvat T, Mahabadi N K, Tsitkov S, Cabelguen J M and Ijspeert A J 2016 From cineradiography to biorobots: an approach for designing robots to emulate and study animal locomotion *J. R. Soc. Interface* **13** 20151089
[49] Krimsky E and Collins S H 2024 Elastic energy-recycling actuators for efficient robots *Sci. Robot.* **9** eadj7246
[50] Lens T, Kirchoff J and von Stryk O 2012 Dynamic modeling of elastic tendon actuators with tendon slackening *IEEE-RAS Int. Conf. on Humanoid Robots* (IEEE) pp 779–84
[51] Liessem S, Held M, Bisen R S, Haberkern H, Lacin H, Bockemühl T and Ache J M 2023 Behavioral state-dependent modulation of insulin-producing cells in *Drosophila Curr. Biol.* **33** 449–463.e5
[52] Lobato-Ríos V, Tata Ramalingasetty S, Gizem Özdil P, Arreguit J, Ijspeert A J and Ramdya P 2022 Neuromechfly, a neuromechanical model of adult *Drosophila melanogaster Nat. Methods* **19** 620–7

[53] Luan H, Diao F, Scott R L and White B H 2020 The *Drosophila* Split Gal4 system for neural circuit mapping *Front. Neural Circuits* **14** 603397
[54] Ma K Y, Chirarattananon P, Fuller S B and Wood R J 2013 Controlled flight of a biologically inspired, insect-scale robot *Science* **340** 603–7
[55] Mamiya A, Gurung P and Tuthill J C 2018 Neural coding of leg proprioception in *Drosophila Neuron* **100** 636–650.e6
[56] Manoonpong P, Patanè L, Xiong X, Brodoline I, Dupeyroux J, Viollet S, Arena P P and Serres J R 2021 Insect-inspired robots: bridging biological and artificial systems *Sensors* **21** 1–44
[57] Mathis A, Mamidanna P, Cury K M, Abe T, Murthy V N, Mathis M W and Bethge M 2018 DeepLabCut: markerless pose estimation of user-defined body parts with deep learning *Nat. Neurosci.* **21** 1281–9
[58] Mettin U, La Hera P X, Freidovich L B and Shiriaev A S 2010 Parallel elastic actuators as a control tool for preplanned trajectories of underactuated mechanical systems *Int. J. Robot. Res.* **29** 1186–98
[59] Moran D T, Chapman K M and Ellis R A 1971 The fine structure of cockroach campaniform sensilla *J. Cell Biol.* **48** 155–73
[60] Murray R M, Li Z and Shankar Sastry S 1994 *A Mathematical Introduction to Robotic Manipulation* 1st edn (CRC Press)
[61] Neher E, Sakmann B and Steinbach J H 1978 The extracellular patch clamp: a method for resolving currents through individual open channels in biological membranes *Pflügers Arch.* **375** 219–28
[62] Ni L 2021 Genetic transsynaptic techniques for mapping neural circuits in *Drosophila Front. Neural Circuits* **15** 749586
[63] Nirody J A 2023 Flexible locomotion in complex environments: the influence of species, speed and sensory feedback on panarthropod inter-leg coordination *J. Exp. Biol.* **226** jeb245111
[64] Nourse W R P, Szczecinski N S and Quinn R D 2023 A synthetic nervous system for on and off motion detection inspired by the *Drosophila melanogaster* optic lobe *Biomimetic and Biohybrid Systems* ed F Meder, A Hunt, L Margheri, A Mura and B Mazzolai (Springer International Publishing) pp 364–80
[65] Park H-W, Wensing P M and Kim S 2017 High-speed bounding with the MIT Cheetah 2: control design and experiments *Int. J. Robot. Res.* **36** 167–92
[66] Phelps J S *et al* 2021 Reconstruction of motor control circuits in adult *Drosophila* using automated transmission electron microscopy *Cell* **184** 759–74
[67] Plooij M, van Nunspeet M, Wisse M and Vallery H 2015 Design and evaluation of the bi-directional clutched parallel elastic actuator (BIC-PEA) *2015 IEEE Int. Conf. on Robotics and Automation (ICRA)* pp 1002–9
[68] Pratt B G, Lee S-Y J, Chou G M and Tuthill J C 2024 Miniature linear and split-belt treadmills reveal mechanisms of adaptive motor control in walking *Drosophila bioRxiv Preprint* https://doi.org/10.1101/2024.02.23.581656 (posted online 24 February 2024, accessed 10 April 2024)
[69] Pratt J and Pratt G 1998 Intuitive control of a planar bipedal walking robot *IEEE Int. Conf. on Robotics and Automation* (IEEE) pp 2014–21
[70] Raibert M, Blankespoor K, Nelson G and Playter R 2008 BigDog, the rough-terrain quadruped robot *IFAC Proc. Vol.* **41** 10822–5
[71] Ramdya P and Ijspeert A J 2023 The neuromechanics of animal locomotion: from biology to robotics and back *Sci. Robot.* **8** 1–14
[72] Ritzmann R E, Quinn R D, Watson J T and Zill S N 2000 Insect walking and biorobotics: a relationship with mutual benefits *BioScience* **50** 23–33
[73] Rosendo A, Nakatsu S, Narioka K and Hosoda K 2013 Pneupard: a biomimetic musculoskeletal approach for a feline-inspired quadruped robot *IEEE Int. Conf. on Intelligent Robots and Systems* (IEEE) pp 1452–7
[74] Rossoni S and Niven J E 2022 Braking slows passive flexion during goal-directed movements of a small limb *Curr. Biol.* **32** 4530–4537.e2
[75] Rubeo S, Szczecinski N S and Quinn R D 2018 A synthetic nervous system controls a simulated cockroach *Appl. Sci.* **8** 6
[76] Santos D, Heyneman B, Kim S, Esparza N and Cutkosky M R 2008 Gecko-inspired climbing behaviors on vertical and overhanging surfaces *IEEE Int. Conf. on Robotics and Automation* pp 1125–31
[77] Saro-Cortes V, Cui Y, Dufficy T, Boctor A, Flammang B E and Wissa A W 2022 An adaptable flying fish robotic model for aero- and hydrodynamic experimentation *Integr. Comp. Biol.* **62** 1202–16
[78] Scharzenberger C, Mendoza J and Hunt A 2019 Design of a canine inspired quadruped robot as a platform for synthetic neural network control *Biomimetic and Biohybrid Systems* ed U Martinez-Hernandez, V Vouloutsi, A Mura, M Mangan, M Asada, T J Prescott and P F M J Verschure (Springer International Publishing) pp 228–39
[79] Scheffer L K and Meinertzhagen I A 2019 The fly brain atlas *Annu. Rev. Cell Dev. Biol.* **35** 637–53
[80] Scheffer L K *et al* 2020 A connectome and analysis of the adult *Drosophila* central brain *eLife* **9** 1–74
[81] Schilling M, Hoinville T, Schmitz J and Cruse H 2013 Walknet, a bio-inspired controller for hexapod walking *Biol. Cybern.* **107** 397–419
[82] Schneider A, Paskarbeit J, Schilling M and Schmitz J 2014 Hector, a bio-inspired and compliant hexapod robot *Biomimetic and Biohybrid Systems* ed A Duff, N F Lepora, A Mura, T J Prescott and P F M J Verschure (Springer International Publishing) pp 427–9
[83] Seelig J D, Eugenia Chiappe M, Lott G K, Dutta A, Osborne J E, Reiser M B and Jayaraman V 2010 Two-photon calcium imaging from head-fixed *Drosophila* during optomotor walking behavior *Nat. Methods* **7** 535–40
[84] Simmering J, Hermes L, Schneider A and Schilling M 2023 Adaptation of a decentralized controller to curve walking in a hexapod robot *Robotics in Natural Settings* ed J M Cascalho, M O Tokhi, M F Silva, A Mendes, K Goher and M Funk (Springer International Publishing) pp 264–75
[85] Sink H 2007 *Muscle Development in Drosophila* 1st edn (Springer)
[86] Soler C, Daczewska M, Da Ponte J P, Dastugue B and Jagla K 2004 Coordinated development of muscles and tendons of the *Drosophila* leg *Development* **131** 6041–51
[87] Spenko M J, Haynes G C, Aaron Saunders J, Cutkosky M R, Rizzi A A, Full R J and Koditschek D E 2008 Biologically inspired climbing with a hexapedal robot *J. Field Robot.* **25** 223–42
[88] Spinola S M and Chapman K M 1975 Proprioceptive indentation of the campaniform sensilla of cockroach legs *J. Comp. Physiol.* A **96** 257–72
[89] Steingrube S, Timme M, Wörgötter F and Manoonpong P 2010 Self-organized adaptation of a simple neural circuit enables complex robot behaviour *Nat. Phys.* **6** 224–30
[90] Steuer J and Pfeiffer F 1997 Control of a six-legged-walking-machine working in uneven terrain *IFAC Proc. Vol.* **30** 97–103
[91] Sutton G P, Szczecinski N S, Quinn R D and Chiel H J 2023 Phase shift between joint rotation and actuation reflects dominant forces and predicts muscle activation patterns *PNAS Nexus* **2** 1–11
[92] Szczecinski N S, Bockemühl T, Chockley A S and Büschges A 2018 Static stability predicts the continuum of interleg coordination patterns in *Drosophila J. Exp. Biol.* **221** jeb.189142
[93] Szczecinski N S, Büschges A and Bockemühl T 2018 *Direction-Specific Footpaths can be Predicted by the Motion*

*of a Single Point on the Body of the Fruit fly Drosophila Melanogaster* (*Lecture Notes in Computer Science* vol 10928 LNAI) (Springer) pp 477–89
[94] Szczecinski N S, Goldsmith C A, Nourse W and Quinn R D 2023 A perspective on the neuromorphic control of legged locomotion in past, present and future insect-like robots *Neuromorph. Comput. Eng.* **3** 023001
[95] Szczecinski N S, Goldsmith C A, Young F R and Quinn R D 2019 Tuning a robot servomotor to exhibit muscle-like dynamics *Biomimetic and Biohybrid Systems* ed U Martinez-Hernandez, V Vouloutsi, A Mura, M Mangan, M Asada, T J Prescott and P F M J Verschure (Springer International Publishing) pp 254–65
[96] Szczecinski N S, Hunt A J and Quinn R D 2017 Design process and tools for dynamic neuromechanical models and robot controllers *Biol. Cybern.* **111** 105–27
[97] Takemura S-Y *et al* 2023 A connectome of the male *Drosophila* ventral nerve cord *bioRxiv Preprint* https://doi.org/10.1101/2023.06.05.543757 (posted online 6 June 2023, accessed 4 June 2024)
[98] Ting L H, Blickhan R and Full R J 1994 Dynamic and static stability in hexapedal runners *J. Exp. Biol.* **197** 251–69
[99] Triantafyllou M S, Triantafyllou G S and Yue D K P 2000 Hydrodynamics of fishlike swimming *Annu. Rev. Fluid Mech.* **32** 33–53
[100] Vantilt J, Giraddi C, Aertbeliën E, De Groote F and De Schutter J 2018 Estimating contact forces and moments for walking robots and exoskeletons using complementary energy methods *IEEE Robot. Autom. Lett.* **3** 3410–7
[101] Venken K J T *et al* 2011 MiMIC: a highly versatile transposon insertion resource for engineering *Drosophila melanogaster* genes *Nat. Methods* **8** 737–47
[102] von Twickel A, Hild M, Siedel T, Patel V and Pasemann F 2012 Neural control of a modular multi-legged walking machine: simulation and hardware *Robot. Auton. Syst.* **60** 227–41
[103] Webb B 2001 Can robots make good models of biological behaviour? *Behav. Brain Sci.* **24** 1033–50
[104] Webb B 2002 Robots in invertebrate neuroscience *Nature* **417** 359–63
[105] Wosnitza A, Bockemühl T, Dubbert M, Scholz H and Büschges A 2013 Inter-leg coordination in the control of walking speed in *Drosophila J. Exp. Biol.* **216** 480–91
[106] Wu X A, Huh T M, Mukherjee R and Cutkosky M 2016 Integrated ground reaction force sensing and terrain classification for small legged robots *IEEE Robot. Autom. Lett.* **1** 1125–32
[107] Zill S N, Büschges A and Schmitz J 2011 Encoding of force increases and decreases by tibial campaniform sensilla in the stick insect, *Carausius morosus J. Comp. Physiol.* A **197** 851–67
[108] Zill S N, Dallmann C J, Zyhowski W P, Chaudhry H, Gebehart C and Szczecinski N S 2024 Mechanosensory encoding of forces in walking uphill and downhill: force feedback can stabilize leg movements in stick insects *J. Neurophysiol.* **131** 198–215
[109] Zill S N and Moran D T 1981 The exoskeleton and insect proprioception III. Activity of tibial campaniform sensilla during walking in the american cockroach, *Periplaneta americana J. Exp. Biol.* **94** 57–75
[110] Zill S N, Ridgel A L, DiCaprio R A and Faith Frazier S 1999 Load signalling by cockroach trochanteral campaniform sensilla *Brain Res.* **822** 271–5
[111] Zyhowski W P, Zill S N and Szczecinski N S 2023 Adaptive load feedback robustly signals force dynamics in robotic model of *Carausius morosus* stepping *Front. Neurorobot.* **17** 1125171